




Article

Rippite, $K_2(Nb,Ti)_2(Si_4O_{12})O(O,F)$, a New K-Nb-Cyclosilicate from Chuktukon Carbonatite Massif, Chadobets Upland, Krasnoyarsk Territory, Russia

Victor V. Sharygin ^{1,2,3,*} , Anna G. Doroshkevich ^{1,4} , Yurii V. Seryotkin ^{1,3} ,
Nikolai S. Karmanov ¹, Elena V. Belogub ^{5,6}, Tatyana N. Moroz ¹, Elena N. Nigmatulina ¹,
Alexander P. Yelisseyev ¹, Vitalii N. Vedenyapin ¹ and Igor N. Kupriyanov ^{1,3}

¹ V.S. Sobolev Institute of Geology and Mineralogy, Siberian Branch of the RAS, 3 Acad. Koptyuga pr., 630090 Novosibirsk, Russia; doroshkevich@igm.nsc.ru (A.G.D.); yuvs@igm.nsc.ru (Y.V.S.); krm@igm.nsc.ru (N.S.K.); moroz@igm.nsc.ru (T.N.M.); helena@igm.nsc.ru (E.N.N.); eliseev@igm.nsc.ru (A.P.Y.); vvn@igm.nsc.ru (V.N.V.); spectra@igm.nsc.ru (I.N.K.)

² ExtraTerra Consortium, Institute of Physics and Technology, Ural Federal University, 19 Mira str., 620002 Ekaterinburg, Russia

³ Department of Geology and Geophysics, Novosibirsk State University, 1 Pirogov str., 630090 Novosibirsk, Russia

⁴ Geological Institute, Siberian Branch of the RAS, 6a Sakhyanova str., 670047 Ulan-Ude, Russia

⁵ South Urals Federal Research Center of Mineralogy and Geoecology, Uralian Branch of the RAS, 456317 Miass, Russia; belogub@mineralogy.ru

⁶ Faculty of Geology, National Research South Ural State University, Miass Branch, 20 8-July str., Bldg. 10, 456304 Miass, Russia

* Correspondence: sharygin@igm.nsc.ru; Tel.: +7-383-330-80-84

Received: 9 November 2020; Accepted: 3 December 2020; Published: 8 December 2020



Abstract: Rippite $K_2(Nb,Ti)_2(Si_4O_{12})O(O,F)_2$, a new K-Nb-cyclosilicate, has been discovered in calciocarbonatites from the Chuktukon massif (Chadobets upland, SW Siberian Platform, Krasnoyarsk Territory, Russia). It was found in a primary mineral assemblage, which also includes calcite, fluorcalciopyrochlore, tainiolite, fluorapatite, fluorite, Nb-rich rutile, olekminskite, K-feldspar, Fe-Mn-dolomite and quartz. Goethite, francolite (Sr-rich carbonate–fluorapatite) and psilomelane (romanèchite ± hollandite) aggregates as well as barite, monazite-(Ce), parisite-(Ce), synchysite-(Ce) and Sr-Ba-Pb-rich keno-/hydropyrochlore are related to a stage of metasomatic (hydrothermal) alteration of carbonatites. The calcite–dolomite coexistence assumes crystallization temperature near 837 °C for the primary carbonatite paragenesis. Rippite is tetragonal: $P4bm$, $a = 8.73885(16)$, $c = 8.1277(2)$ Å, $V = 620.69(2)$ Å³, $Z = 2$. It is closely identical in the structure and cell parameters to synthetic $K_2Nb_2(Si_4O_{12})O_2$ (or $KNbSi_2O_7$). Similar to synthetic phase, the mineral has nonlinear properties. Some optical and physical properties for rippite are: colorless; Mohs' hardness—4–5; cleavage—(001) very perfect, (100) perfect to distinct; density (meas.)—3.17(2) g/cm³; density (calc.)—3.198 g/cm³; optically uniaxial (+); $\omega = 1.737$ –1.739; $\epsilon = 1.747$ (589 nm). The empirical formula of the holotype rippite (mean of 120 analyses) is $K_2(Nb_{1.90}Ti_{0.09}Zr_{0.01})[Si_4O_{12}](O_{1.78}OH_{0.12}F_{0.10})$. Majority of rippite prismatic crystals are weakly zoned and show Ti-poor composition $K_2(Nb_{1.93}Ti_{0.05}Zr_{0.02})[Si_4O_{12}](O_{1.93}F_{0.07})$. Raman and IR spectroscopy, and SIMS data indicate very low H₂O content (0.09–0.23 wt %). Some grains may contain an outermost zone, which is enriched in Ti (+Zr) and F, up to $K_2(Nb_{1.67}Ti_{0.32}Zr_{0.01})[Si_4O_{12}](O_{1.67}F_{0.33})$. It strongly suggests the incorporation of (Ti,Zr) and F in the structure of rippite via the isomorphism $Nb^{5+} + O^{2-} \rightarrow (Ti,Zr)^{4+} + F^{1-}$. The content of a hypothetical end-member $K_2Ti_2[Si_4O_{12}]F_2$ may be up to 17 mol. %. Rippite represents a new structural type among $[Si_4O_{12}]$ -cyclosilicates because of specific type of connection of the octahedral

chains and $[\text{Si}_4\text{O}_{12}]^{8-}$ rings. In structural and chemical aspects it seems to be in close with the labuntsovite-supergroup minerals, namely with vuoriyarvite-(K), $\text{K}_2(\text{Nb,Ti})_2(\text{Si}_4\text{O}_{12})(\text{O,OH})_2 \cdot 4\text{H}_2\text{O}$.

Keywords: rippite; new mineral; K-Nb-cyclosilicate; synthetic $\text{K}_2\text{Nb}_2(\text{Si}_4\text{O}_{12})\text{O}_2$; calciocarbonatite; Chuktukon massif; Chadobets upland; Krasnoyarsk Territory

1. Introduction

The natural analog of the tetragonal synthetic phase KNbSi_2O_7 , a new structural type among natural K-Nb-cyclosilicates, named rippite, was discovered in calciocarbonatites of the Chuktukon massif, Chadobets upland, SW Siberian Platform, Krasnoyarsk Territory, Russia [1,2].

Synthetic $\text{K}_2\text{Nb}_2(\text{Si}_4\text{O}_{12})\text{O}_2$ (or KNbSi_2O_7) is actively studied since 1990 [3]. The melting point for $\text{K}_2\text{Nb}_2(\text{Si}_4\text{O}_{12})\text{O}_2$ is 1180 °C. No phase transition was found in $\text{K}_2\text{Nb}_2(\text{Si}_4\text{O}_{12})\text{O}_2$ between room temperature and melting point [4]. It is rather inert and chemically stable and is not dissolved in inorganic acids except HF. All studies on KNbSi_2O_7 are mainly focused on its nonlinear optical property [3–15]. Single crystals, ceramics, glass-ceramics, and glass of KNbSi_2O_7 and similar compositions in the systems $\text{SiO}_2(\pm\text{GeO}_2)\text{-Nb}_2\text{O}_5\text{-K}_2\text{O}$ have been fabricated [3–12]. The synthesis of glasses and glass-ceramics in the system $\text{SiO}_2\text{-Nb}_2\text{O}_5\text{-K}_2\text{O}$ has shown that $\text{K}_2\text{Nb}_2(\text{Si}_4\text{O}_{12})\text{O}_2$ may be appeared in the 510–735 °C temperature range in glass/melt [4,6,8–10,13,14]. The KNbSi_2O_7 phase has very high optical nonlinearity with its second harmonic generation (SHG) signal greater than that for α -quartz [14,15]. The study of ferroelectric-dielectric properties has shown that $\text{K}_2\text{Nb}_2(\text{Si}_4\text{O}_{12})\text{O}_2$ is a ferroelectric material with low dielectric permittivity range [4,14]. The isostructural compound $\text{K}_2\text{Ta}_2(\text{Si}_4\text{O}_{12})\text{O}_2$, which may has nonlinear properties, was also synthesized [16].

Rippite, $\text{K}_2(\text{Nb,Ti})_2(\text{Si}_4\text{O}_{12})\text{O}(\text{O,F})$, was approved by the Commission on New Minerals, Nomenclature and Classification (CNMNC) of the International Mineralogical Association (IMA) as a new mineral species in June 2016 (IMA 2016-025) [1]. The mineral is named in the honor of German Samuilovich Ripp (1935 year of birth, Ulan-Ude, Buryatia, Russia). He is a leading expert on carbonatite petrogenesis, including carbonatite magmatic activity in Eastern Siberia, carbonatite mineralogy, geochemistry and stable isotope geochemistry and rare metal mineralization associated with carbonatites. He has performed detailed studies for carbonatite occurrences in Transbaikalia (Yuzhnoe, Khaluta, Arshan, Pogranichnoe, Veseloe), Eastern Sayan (Belaya Zima) and Mongolia (Mushugai-Khuduk) [17–28]. The holotype specimen of rippite-containing carbonatite from drillhole N 546 (193.5 m deep, author number 546–193.5) of the Chuktukon massif, Siberia, Russia has been deposited in the Central Siberian Geological Museum at the V.S. Sobolev Institute of Geology and Mineralogy (IGM), Siberian Branch of the RAS, Novosibirsk 630090, Russia, catalogue number XIII-347/1).

In this paper, we provide a detailed description of rippite. Some data on rippite-bearing calciocarbonatites of the Chuktukon massif were reported in the previous publications [1,2,29–35].

2. Brief Geological Background for the Chuktukon Massif

The Chadobets alkaline complex is located within the Chadobets upland (basin of the Chadobets River, Krasnoyarsk Territory, Russia) at the southwestern part of the Siberian craton (Figure 1) [36]. The upland is 2000 km² in size and occurs at the intersection of two Neoproterozoic grabens being a part of the Angara-Kotuy large-scale rift system [29,37–39]. The Chadobets alkaline ultramafic carbonatite complex is conventionally subdivided into the Chuktukon alkaline ultramafic carbonatite massif (southern part of the upland) and the Terina alkaline massif (silicate rocks, northern part of the upland). In addition, the Chadobets upland also includes dikes of ultramafic lamprophyres (aillikite–damtjernite series). Carbonatites and their weathering species of the Chuktukon massif host major reserves of Nb and REE [40–42]. The U-Pb and Ar-Ar ages for the Chadobets ultramafic alkaline rocks and

carbonatites are between 252 and 231 Ma [30,31,43]. For comparison, the Ilbokich aillikite–damtjernite lamprophyre series, which is located nearby the Chadobets upland, has 392 Ma age [43–45].

The detailed geology of the Chadobets alkaline ultramafic carbonatite complex was described by Kirichenko et al. [36]. The sequence of the Chuktukon rocks, from the earliest to the youngest, was established by field observations (drillholes description) and comprises alkaline ultramafic rocks, calciocarbonatites and, finally, damtjernites [36]. Alkaline ultramafic rocks (aillikites–damtjernites, olivine melilitites, peridotites and others) of the first emplacement phase form small plugs (up to 1–1.5 km²), dykes and sills ranging in thickness up to 100–120 m. Carbonatites also form small plugs (up to 4 km²), dykes and sills (up to 20 m thick). Damtjernites are presented by pipes (up to 0.5 km²), crosscutting early phases of alkaline ultramafic rocks and carbonatites and typically containing their xenoliths and fragments of the country sedimentary rocks. All rocks of the Chuktukon massif are altered in different degree by hydrothermal and weathering processes [36]. The detailed petrography and mineralogy of the Chadobets alkaline rocks were summarized in [29,30,32,36,43,46,47].

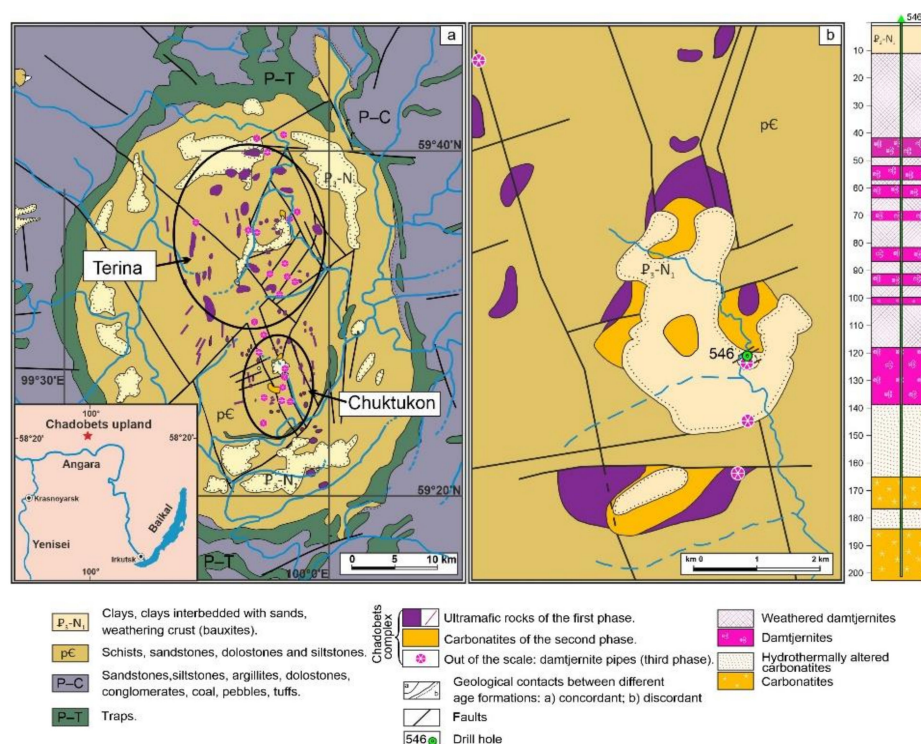


Figure 1. (a) Geological scheme of the Chadobets upland and (b) the Chuktukon massif within the upland and cross-section for the 546 drillhole ([36] and unpublished data from geological report of “Krasnoyarskgeols’emka”, 2010).

3. Analytical Methods

Double-polished sections of calciocarbonatites (~50–100 µm in thickness) and individual rippite grains from the Chuktukon massif were used for optical examination in transmitted and reflected light and for other studies. The individual rippite crystals were selected from residue after dissolution of carbonatite samples in the diluted HCl or acetic acid.

The identification of all minerals in the Chuktukon calciocarbonatites was based on energy-dispersive spectra (EDS), back-scattered electron (BSE) images and elemental mapping (EDS system), using a TESCAN MIRA 3MLU scanning electron microscope equipped with an INCA Energy 450 XMax 80 microanalysis system (Oxford Instruments Ltd., Abingdon, UK) at the IGM, Novosibirsk, Russia. The SEM-EDS analyses of minerals were operated at an accelerating voltage of 20 kV and a probe current of 1 nA in high-vacuum mode and at an accumulation time of 20–40 s.

The synthetic compounds, pure metals and minerals were used as reference standards for the elements: SiO₂ (Si and O), Al₂O₃ (Al), diopside (Mg and Ca), albite (Na), orthoclase (K), Ca₂P₂O₇ (P), BaF₂ (Ba and F), Cr₂O₃ (Cr), CsRe₂Cl₆ (Cl), LaPO₄ (La), CePO₄ (Ce), SrF₂ (Sr), metallic Nb, Ti, Ta, Zr, Fe, Mn, Zn and V. Matrix effects were corrected using the XPP algorithm, implemented in the software of the microanalysis system. Metallic Co served for quantitative optimization (normalization to probe current and energy calibration of the spectrometer).

Electron microprobe analyses (EMPA-WDS) of rippite and related carbonatite minerals were done at the IGM, using a JEOL JXA-8100 electron microprobe (Jeol Ltd., Tokyo, Japan). Grains (sizes >5 µm) previously analyzed by SEM-EDS were selected for this purpose. The operating conditions were as follows: beam diameter of 1–2 µm, accelerating voltage of 20 kV and a beam current of 10–15 nA, counting time of 10 (5 + 5) s (for most elements). Accumulation time for analyzing of F (using LDE crystal) in rippite was 40 s (20 s—counting of background; 20 s—counting of peak for F), detection limit for F was 308 ppm (0.03 wt %). Synthetic fluorophogopite (Si, Al, F, Mg), orthoclase (K), LiNbO₃ (Nb), zircon (Zr), rutile (Ti), Ta₂O₅ (Ta), diopside (Ca), Fe-rich pyrope (Fe), Ba-silicate glass (Ba), Sr-silicate glass (Sr) and albite (Na) were used as standards during measuring. The precision of analysis for major elements was better than 2% relative. The detection limits for elements were (in ppm): Si—181; Ti—132; Nb—295; Zr—405; Ta—400; Al—168; Fe—28; Mg—188; Ca—123; Sr—844; Na—128; K—115. Data reduction was performed using a PAP routine (Pouchou & Pichoir, 1985). Overlap corrections were done for the following elements: SiK α —SrL α , SiK α —TaM α and FeL α —FK α .

The contents of some light trace elements (Be, Li, B), F and H₂O in rippite of the Chuktukon carbonatite were analyzed by secondary-ion mass spectrometry (SIMS) on a Cameca IMS-4f ion probe at the Analytical Centre of the Yaroslavl Branch of the Institute of Physics and Technology (YBIPT), Yaroslavl, Russia. For the analysis, grains larger than 20 µm and previously analyzed by EMPA-WDS and SEM-EDS were selected. Analysis of trace elements was carried out by the energy filter method; the operating conditions were as follows: primary O^{2−} beam—20 µm, $I = 2\text{--}4$ nA, energy offset—100 eV, and energy slit—50 eV. Concentrations of elements were determined from the ratios of their isotopes to ³⁰Si, using calibration curves for standard samples [48]. The hydrogen content was determined from the ¹H mass together with trace elements. Low background content of H₂O (0.03 wt %) in the mass spectrometer was achieved by storing the samples for 24 h in high-vacuum. The NIST SRM610 glass was used as external standard [49].

The trace element composition of rippite was also determined by laser ablation ICP-MS at the Friedrich-Alexander University, Erlangen-Nürnberg, Germany. The instrumentation includes an Agilent 7500i inductively coupled plasma mass spectrometer combined with an ESI New Wave UP193-FX laser ablation system. Samples were ablated at plasma power of 1350 W in an atmosphere of pure He (0.65 L/min) and Ar (1.10 L/min) as gas carriers. In addition, Ar was used as the plasma (14.9 L/min) and auxiliary gas (0.9 L/min) plasma immediately after the ablation cell. Analyses were conducted in spot mode, each analysis lasting 80 s, including 20 s of background acquisition (laser off) followed by 60 s of ablation. A beam 10–50 µm in diameter (2.7 J/cm²) with a laser frequency of 16 Hz was used. The NIST SRM610 standard [49] was used to calibrate the weights of determined elements. The contents of minor elements were compared to those measured on an electron microprobe. Trace element concentrations were calculated with the GLITTER software [50].

The Raman spectra for rippite were recorded on a LabRAM HR 800 mm (HORIBA Scientific Ltd., Kyoto, Japan) spectrometer equipped with a 1024 pixel LN/CCD detector and coupled to an Olympus BX40 confocal microscope (objective $\times 100$) at the IGM. A semiconductor laser emitting at 514.5 nm with a nominal power output of 50 mW was used for excitation. In each case, a 200 µm confocal hole and integrated. Most spectra were recorded between 100 and 1200 cm^{−1}, and some spectra were made for the 100–4000 cm^{−1} and 3000–4000 cm^{−1} region. The monochromator was calibrated using the 520.7 cm^{−1} Raman line of elemental Si. A Bruker Vertex 70 FTIR spectrometer equipped with a Hyperon 2000 microscope at the IGM was used for measurements of rippite in the IR region (powder KBr pellets and individual crystals putted on KBr plate). Pellets for infrared absorbance measurements

were obtained by pressing a mixture of about 1 mg of powdered rippite diluted in 400 mg of dried KBr. Spectra over $4000\text{--}370\text{ cm}^{-1}$ range were obtained by of 23 scans with a resolution of 2 cm^{-1} . Interferences from KBr and air were cancelled by subtracting their spectra from the sample spectrum.

The second harmonic generation test (non-linear properties) were provided for rippite using diode pumped solid-state laser DTL-399QT (laser YLF:Nd³⁺; pulse duration—7–10 ns; energy—100 microjoule; focusing with 50 mm lens; basic frequency 1052 nm was separated by IRG-3 filter) at the IGM. A JSM 6510 LV scanning microscope equipped with Gatan Chrome CL 4UV at the IGM was used for the cathodoluminescence (CL) images ($V = 10\text{ kV}$, quality 1024×1024) of rippite.

Crystallographic studies of rippite were done at Novosibirsk State University, Novosibirsk, Russia. X-ray powder diffraction data were collected using Stoe IPDS 2T diffractometer (MoK α , $\lambda = 0.71073\text{ \AA}$, Gandolfi geometry). Single-crystal X-ray studies were carried out using an Oxford Diffraction Xcalibur Gemini diffractometer (MoK α , $\lambda = 0.71073\text{ \AA}$).

The main results are presented in Figures 1–15 and Tables 1–9. Some data are given in Supplementary section (Table S1 and Figures S1–S7).

4. Mineralogy and Petrography of Calciocarbonatites from the Chuktukon Massif

The Chuktukon calciocarbonatites are fine- and medium-grained rocks with massive, spotty and banded textures (Figure 2), sometimes contain vugs which are filled with euhedral calcite, barite and/or quartz. Some species are medium to highly altered. The primary mineral assemblage includes calcite, fluorcalciopyrochlore, rippite, tainiolite, fluorapatite (up to 2.3 wt % SrO), fluorite, Nb-rich rutile (up to 17 wt % Nb₂O₅, up to 5.1 wt % Fe₂O₃), K-feldspar, dolomite, ancylite-(Ce), strontianite, olekminskite, sulfides, aegirine, quartz and zircon. Calcite is speckled with dolomite spots and fine disseminations of ancylite-(Ce), strontianite, and olekminskite. The SrO concentration in calcite is up to 0.8 wt % [29]. Minerals found in all species of calciocarbonatites are listed in Table 1. The chemical compositions of some minerals are considered in previous works [1,2,29–35]. In general, rippite is the second main mineral to concentrate Nb in the Chuktukon calciocarbonatites [1,2,29,32], and its content in some rocks may be equal and even higher rather than that of pyrochlore.

Strontianite, daqingshanite-(Ce), ferrohagendorffite, barite, burbankite–khanneshite, Na-Ca carbonates (nyerereite, shortite), thorite, anhydrite, hematite, baddeleyite, zirconolite-group minerals, unidentified Na-REE-Ba-Sr-Ca-rich and Na-Fe-rich phosphates, and Na-rich hydrated carbonate occasionally appear in multiphase or monomineralic inclusions in fluorapatite, fluorcalciopyrochlore, zircon and calcite of the Chuktukon calciocarbonatites [30,34,35]. The secondary multiphase inclusions from the cores of zircon are carbonate-rich in composition and multiphase: calcite + dolomite or alkali-rich carbonates (nyerereite + shortite + burbankite) [30,34].

Aggregates of “francolite” (Sr-rich carbonate-fluorapatite with up to 7 wt % SrO), “goethite” (goethite + “hydrogoethite” \pm other Fe-oxides/hydroxides) and “psilomelane” (romanèchite \pm hollandite) are common in various quantities for all calciocarbonatite species (Figure 2). Barite, quartz, Ca-REE-fluorcarbonates (parisite-(Ce), synchysite-(Ce)), monazite-(Ce), Sr-Ba-Pb-rich hydro-/kenopyrochlores and above aggregates are related to a stage of metasomatic (hydrothermal) alteration of the calciocarbonatites. They occur interstitially among grains of primary minerals and/or form networks of microveinlets. In addition, goethite forms complete pseudomorphs after euhedral pyrite and prismatic grains (up to 1 cm) of an unidentified mineral, which commonly contains inclusions of calcite and tainiolite (Figure 2) [33].

Detailed studies of the petrography and mineralogy of the highly altered calciocarbonatite are given in [32,40]. These rocks are composed of relict minerals (calcite, fluorcalciopyrochlore, rippite, rutile, and zircon) and minerals formed during alteration. The rocks are fine-grained, banded, and patchy-striped, which is expressed as alternating bands and spots of goethite and rare earth minerals. The groundmass is composed of an aggregate of “goethite” and kaolinite. Florencite-(Ce), monazite-(Ce), “psilomelane” aggregate, churchite-(Y), and daqingshanite-(Ce) are minor and accessory minerals.

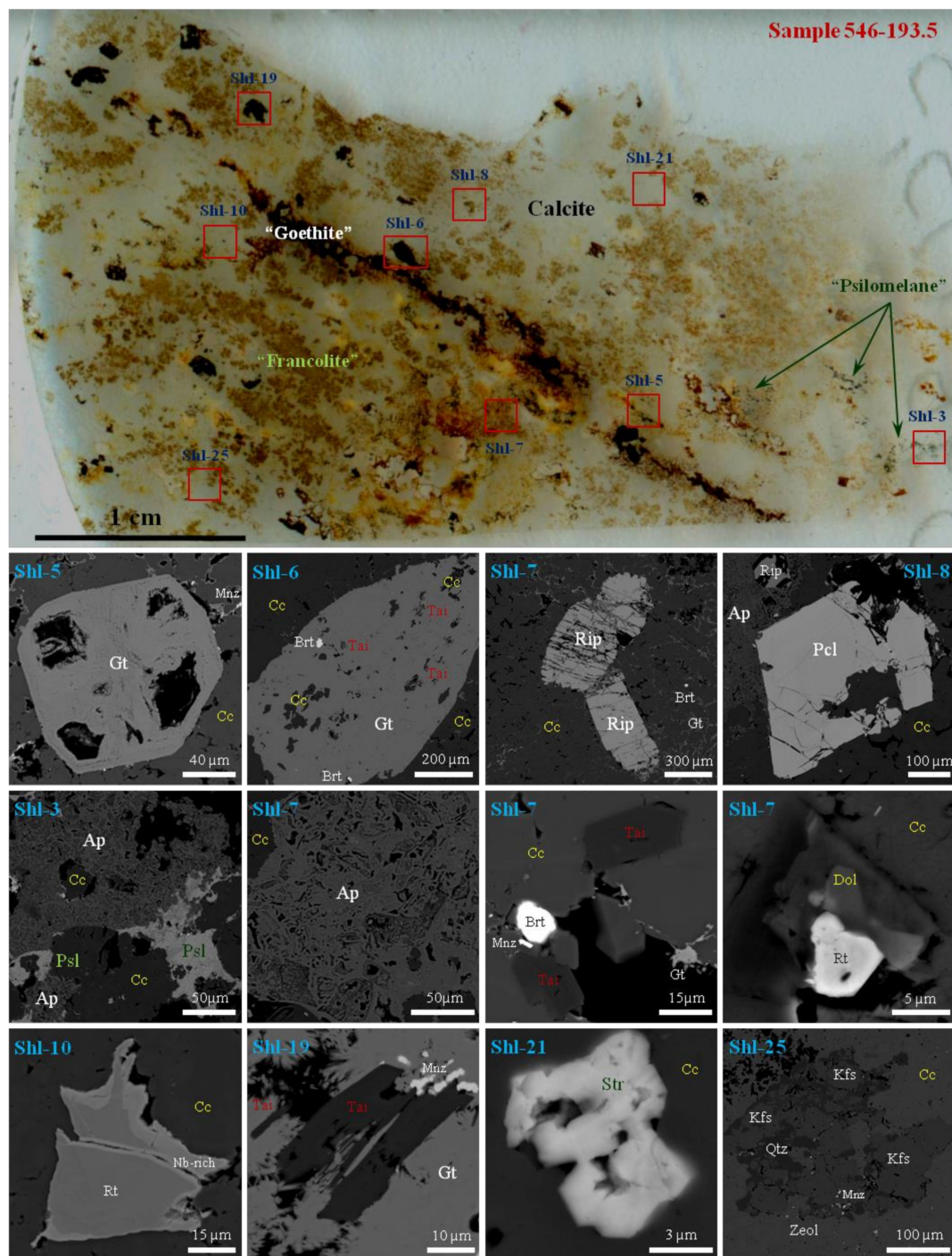


Figure 2. General view and mineral relations for calciocarbonatite from the Chuktukon massif (holotype sample for rippite, 546-193.5), ordinary light and back-scattered electron (BSE) images. Symbols: "Goethite", Gt—aggregate of goethite and other Fe-oxy/hydroxides; "Francolite", Ap—Sr-rich carbonate-fluorapatite; "Psilomelane", Psl—psilomelane aggregate (romanèchite + hollandite + others); Cc—calcite; Mnz—monazite-(Ce); Tai—tainiolite; Brt—barite; Rip—rippite; Pcl—fluorcalciopyrochlore; Dol—Fe-Mn-rich dolomite; Rt—rutile (Nb_2O_5 —2.2–14.7 wt %; Fe_2O_3 —0.3–3.9 wt %); Str—strontianite; Kfs—K-feldspar; Qtz—quartz; Zeol—K-Ca-zeolite (?).

"Goethite" aggregate from hydrothermally altered carbonatites contains up to 2.2 wt % of Nb_2O_5 [32]. Florencite-(Ce) and monazite-(Ce) occur as irregularly shaped grains, up to 0.3 cm in size, as well as aggregates of micron-sized grains of intricately shaped patches, as well as network

of vein-like segregations. Typically, both minerals have a porous internal structure. Churchite-(Y) forms radially fibrous 2–5 mm aggregates and individual 2–3 mm crystals. A network of “psilomelane” (microveinlets) dissects the rocks [29]. The petrographic observations of different types of the Chuktukon calciocarbonatites have shown that rippite is very resistant to alteration/weathering processes. In addition to holotype sample 546–193.5 (Figure 2) this mineral was also found as minor component in calciocarbonatites (including highly altered samples) from 180–200 m depths of neighboring drillholes.

Table 1. List of minerals found in the Chuktukon calciocarbonatites.

Mineral	Formula	Mineral	Formula
Pyrite	FeS ₂	Ancylite-(Ce)	(Ce,La,Nd)Sr(CO ₃) ₂ (OH) H ₂ O
Fluorite	CaF ₂	Daqingshanite-(Ce)	(Sr,Ca,Ba) ₃ (Ce,La)(CO ₃) _{3-x} (PO ₄)(OH,F) _{2x}
Neighborhoodite	NaMgF ₃	Quartz	SiO ₂
Parascandolaite	KMgF ₃	Rutile	TiO ₂
Fluorapatite	Ca ₅ (PO ₄) ₃ F	Baddeleyite	ZrO ₂
Carbonate-fluorapatite	(Ca,Sr,Na) ₅ (PO ₄ ,CO ₃) ₃ F	Thorianite	ThO ₂
Monazite-(Ce)	(Ce,La,Nd)PO ₄	Hematite	Fe ₂ O ₃
Ferrohagendorfite	NaCaFe ²⁺ Fe ²⁺ ₂ (PO ₄) ₃	Laachite	Ca ₂ Zr ₂ Nb ₂ TiFe ²⁺ O ₁₄
Florencite-(Ce)	(Ce,La,Nd)Al ₃ (PO ₄) ₂ (OH) ₆	“Nb-Fe ³⁺ -zirconolite”	Ca ₂ Zr ₂ NbTi ₂ Fe ³⁺ O ₁₄
“Sr-Ba-Ca-Na-REE-phosphate”	(Na,REE)Ca _{2.5} (Sr,Ba) ₃ (PO ₄) ₄ (OH)	Fluorcalciopyrochlore	(Ca,Na) ₂ (Nb,Ti) ₂ O ₆ F
“Na-Ca-Fe-Mn-phosphate”	Na _{4.8} Ca _{0.6} (Fe,Mn) ₃ (PO ₄) ₄	Hydroxykenopyrochlore	(□,Ce,Ba) ₂ (Nb,Ti) ₂ O ₆ (OH,F)
“Na-REE-Ca-Sr-Ba-phosphate”	Na _{1.6} REE _{0.6} (Ba,Sr,Ca) _{0.8} (PO ₄)O	Hydropyrochlore	(H ₂ O,Ba,Sr,□) ₂ Nb ₂ (O,OH) ₆ (H ₂ O)
“Ba-Sr-Ca-REE-H ₂ O-aluminophosphate”	(Ba,Sr,Ca,REE)Al(PO ₄) _n H ₂ O	Hydroxylumbo-pyrochlore	(Pb _{1.5} □ _{0.5})Nb ₂ O ₆ (OH)
Churchite-(Y)	Y(PO ₄) ₂ H ₂ O	Goethite	α-FeOOH
Anhydrite	CaSO ₄	“Hydrogoethite”	3Fe ₂ O ₃ ·4H ₂ O
Barite	BaSO ₄	Bernalite	Fe(OH) ₃ nH ₂ O
Celestine	SrSO ₄	Ferrihydrite	Fe ³⁺ ₁₀ O ₁₄ (OH)
Calcite	CaCO ₃	Hollandite	Ba(Mn ⁴⁺ ₆ Mn ³⁺ ₂)O ₁₆
Strontianite	SrCO ₃	Romanèchite	(Ba,H ₂ O) ₂ (Mn ⁴⁺ ₆ Mn ³⁺ ₂)O ₁₀
Dolomite	CaMg(CO ₃) ₂	K-feldspar	KAlSi ₃ O ₈
Ankerite	Ca(Fe ²⁺ ,Mg,Mn)(CO ₃) ₂	Diopside	CaMgSi ₂ O ₆
Olekminskite	Sr(Sr,Ca,Ba)(CO ₃) ₂	Aegirine	NaFe ³⁺ Si ₂ O ₆
Nyerereite	Na ₂ Ca(CO ₃) ₂	Tainiolite	KMg ₂ Li(Si ₃ O ₁₀)F ₂
Shortite	Na ₂ Ca ₂ (CO ₃) ₃	Rippite	K ₂ (Nb,Ti) ₂ (Si ₄ O ₁₂)O(O,F)
Synchysite-(Ce)	Ca(Ce,La,Nd)(CO ₃) ₂ F	Zircon	ZrSiO ₄
Parasite-(Ce)	Ca(Ce,La,Nd) ₂ (CO ₃) ₃ F ₂	Thorite	ThSiO ₄
Burbankite	(Na,Ca) ₃ (Sr,Ba,Ce) ₃ (CO ₃) ₅	Kaolinite	Al ₂ (Si ₂ O ₅)(OH) ₄
Khanneshite	(Na,Ca) ₃ (Ba,Sr,Ce,Ca) ₃ (CO ₃) ₅	“K-Ca-zeolite”	K ₃ Ca ₅ (Al ₃ Si ₉ O ₂₉)·7–8H ₂ O

New author’s data and data from [1,2,29–35] were used. The names in inverted commas mean poorly identified phases.

5. Morphology, Optical and Physical Properties of Rippite

Rippite commonly forms elongated prismatic crystals (up to 0.5–2 mm) and their intergrowths in carbonate matrix (Figures 2 and 3), rarely in the “goethite” or “francolite” aggregates. The major forms are prism {100} and pinacoid {001}. Twinning is none observed. The mineral is colorless and it may be confused with fluorapatite due to elongated crystals.

The color of the powdered mineral is white. Rippite has vitreous luster and weak fluorescence. The second harmonic generation test indicated nonlinear optical properties of the mineral. Under laser the weak glow of rippite powder was steady and green that was comparable with colour characteristics of the reference sample (LiIO₃). Cleavage is very perfect on (001) and perfect to distinct on (100); parting is none observed, fracture is stepped to uneven across cleavage (Figure 3). The Mohs’ hardness of rippite is 4–5, micro-indentation hardness is VHN₅₀ = 210–487 kg/mm², mean (n = 19)—307 kg/mm². The density measured by flotation in the Clerici liquid (HCOOTl + Tl₂[OOCCH₂COO]) is 3.17(2) g/cm³. Density calculated from unit-cell dimensions and results of electron-microprobe analyses assumes 3.198 g/cm³. Rippite is optically uniaxial (+); ω = 1.737–1.739; ε = 1.747 (589 nm). The optical orientation is X = c. No dispersion and pleochroism were observed. The mineral is not soluble in concentrated

HCl and H_2SO_4 that is comparable with the synthetic phase. The Gladstone–Dale’s compatibility factor for the holotype rippite is 0.005 (superior).

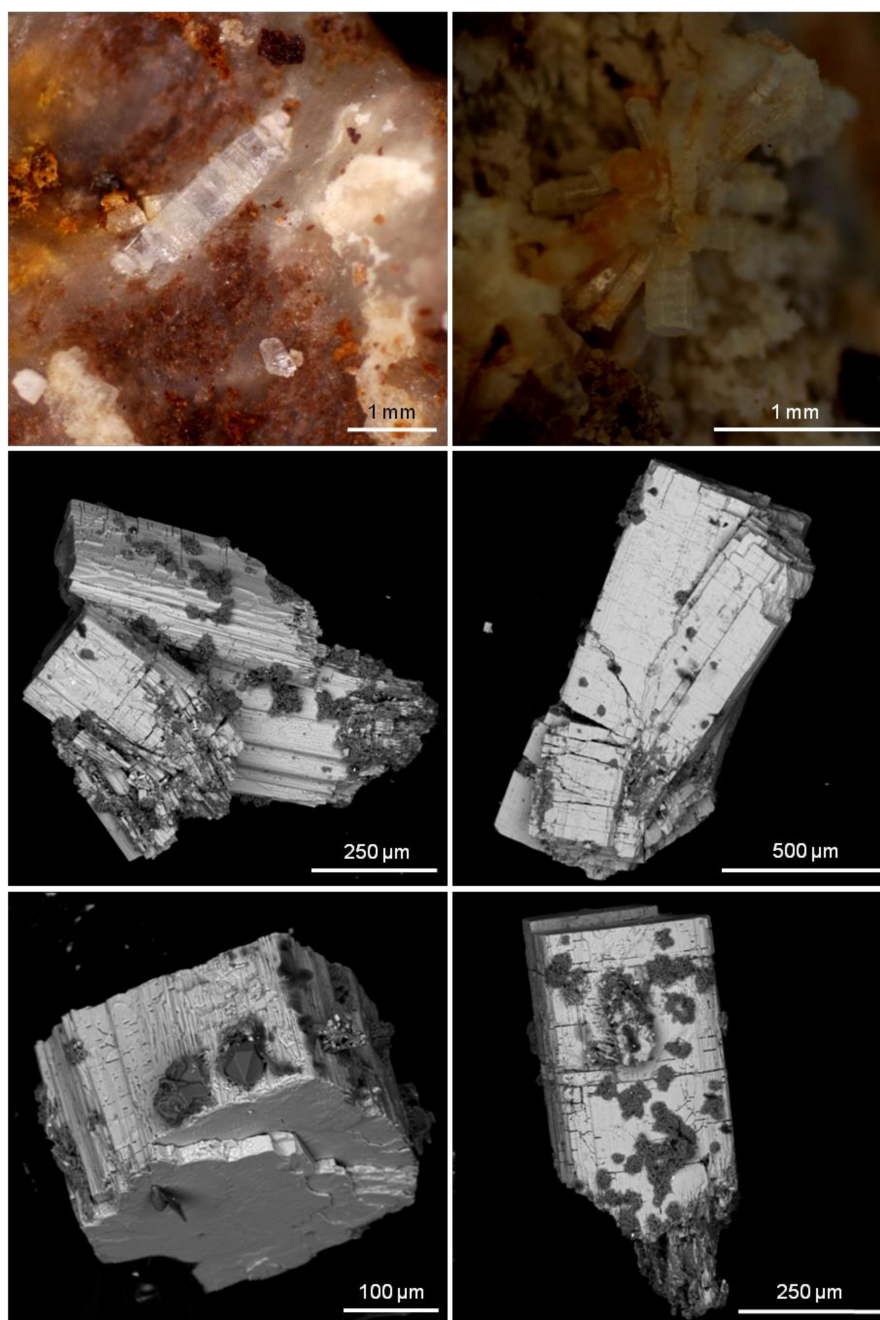


Figure 3. Discrete crystal fragments and intergrowths of rippite from the Chuktukon calciocarbonatite, ordinary light and BSE images (holotype sample 546–193.5). The rock fragments were partially or completely dissolved by diluted HCl acid. Some faces of rippite crystals are partially covered by quartz.

Fluorcalciopyrochlore octahedra and tainiolite blades occasionally occur as inclusions in rippite, and vice versa rippite (\pm quartz and other phases) sometimes fills the fissures in fluorcalciopyrochlore crystals (Figure 4, Figures S1 and S2). Such relationships indicate that rippite is later Nb-mineral than fluorcalciopyrochlore and crystallized together with tainiolite or later (Figure 4, Figures S1–S3). Most of rippite grains are partially resorpted by quartz especially along cleavage planes and even replaced by quartz in the outer parts of some crystals (Figures 3–5, Figures S3–S5). “Goethite” impregnation is

common of some grains occurring in altered carbonatite samples. In general, rippite is resistant to low-temperature alteration or weathering, but may be partially replaced by quartz (plus rutile and other phases) during carbonatite crystallization (Figure 5 and Figures S3–S5).

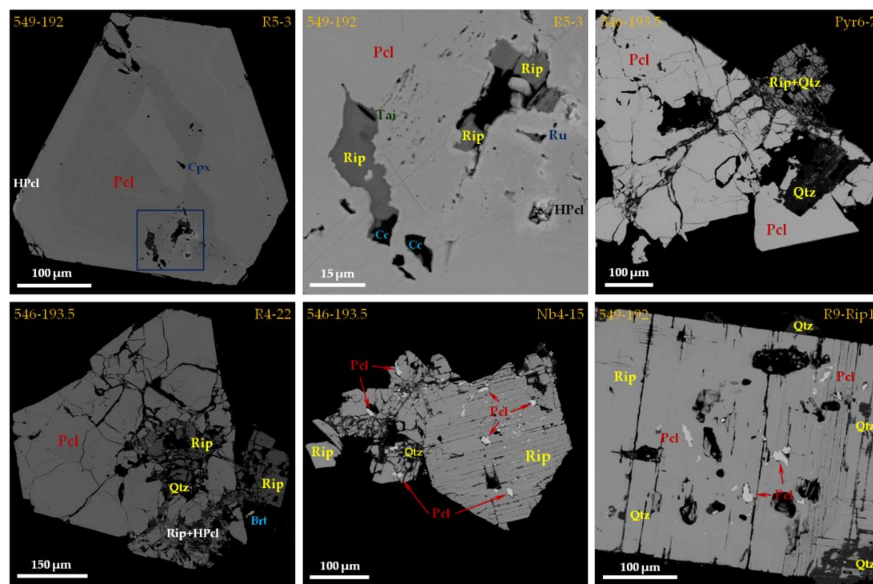


Figure 4. Relations between fluorcalciopyrochlore and rippite in the Chuktukon calciocarbonatites, BSE images. Symbols: Rip—rippite; Pcl—fluorcalciopyrochlore; HPcl—Ba-Sr-Pb-rich hydro-/kenopyrochlore; Cpx—Ca-Na-rich clinopyroxene; Cc—calcite; Ru—rutile; Tai—tainiolite; Qtz—quartz; Brt—barite. For some details see Figures S1 and S2.

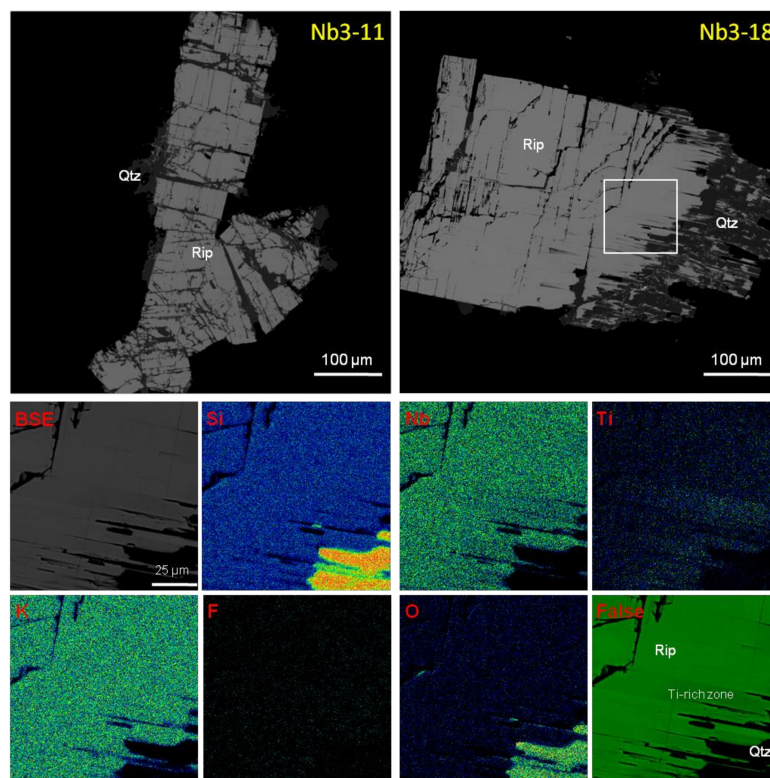


Figure 5. Rippite crystals partially resorbed by quartz (BSE images) and elemental maps for area with Ti-rich composition (holotype sample 546-193.5). Rip—rippite; Qtz—quartz.

6. Chemical Composition of Rippite

6.1. SEM and EMPA Data

Majority of rippite prismatic crystals are homogeneous in composition and unzoned or weakly-zoned that is virtually invisible in the elemental SEM maps (Figures S3, S6 and S7). The contrast zonation is only fixed for rare grains with narrow Ti-rich outermost zone. Those core-to-rim variations are well indicated in the Nb and Ti elemental maps (Figure 5). In general the chemical composition of the mineral is close to the ideal structural formula $K_2Nb_2(Si_4O_{12})O_2$ (Tables 2 and 3). The empirical formula of the holotype rippite (sample 546-193.5, mean of 110 analyses) is $K_2(Nb_{1.90}Ti_{0.09}Zr_{0.01})[Si_4O_{12}](O_{1.78}OH_{0.12}F_{0.10})$ (Table 2). Most of grains from holotype and other samples show compositions poor in TiO_2 (<0.7–1.0 wt %) and F (<0.5 wt %), $K_2(Nb_{1.93}Ti_{0.05}Zr_{0.02})[Si_4O_{12}](O_{1.93}F_{0.07})$ (Tables 2 and 3). Raman, IR and SIMS data indicate very low content of H_2O or (OH)-groups in such grains (see text below). High contents of TiO_2 (up to 4.4 wt %) and F (up to 1.0 wt %) are common of the outermost zone in some grains, up to $K_2(Nb_{1.67}Ti_{0.32}Zr_{0.01})[Si_4O_{12}](O_{1.67}F_{0.33})$ (Table 2, Figure 5). The ZrO_2 amount is up to 1.3 wt %. However, there is no any clear correlation ZrO_2 with TiO_2 and Nb_2O_5 (Figure 6). All above-mentioned data strongly suggest the incorporation of (Ti,Zr) and F in the structure of rippite via the isomorphism $Nb^{5+} + O^{2-} \rightarrow (Ti,Zr)^{4+} + F^{1-}$ (Figure 7). The content of a hypothetical end-member $K_2Ti_2[Si_4O_{12}]F_2$ may be up to 17 mol. % (Table 2). The database of chemistry for all rippite grains is given in Supplementary Table S1.

6.2. LA-ICP-MS and SIMS Data

Trace elements were measured by LA-ICP-MS for Ti-poor compositions of rippite from the Chuktukon calciocarbonatite. The REE and trace element concentrations are consistently low (<220 ppm in total) (Table 4). The substantial amounts (>2–5 ppm) are common of P (22–23 ppm), Ca (16 ppm), Ba (153–205 ppm), V (12–26 ppm), Sc (7.1–9.4 ppm), Hf (22–36 ppm) and Ta (7.3–11.3 ppm) (Table 4).

The contents of some light trace elements (Be, Li, B), F and H_2O in low-Ti rippite were analyzed by SIMS (Table 4). The results indicate very low concentration of light elements (<5 ppm) and H_2O (0.09–0.23 wt %). The content of F is consistent with EMPA-WDS data.

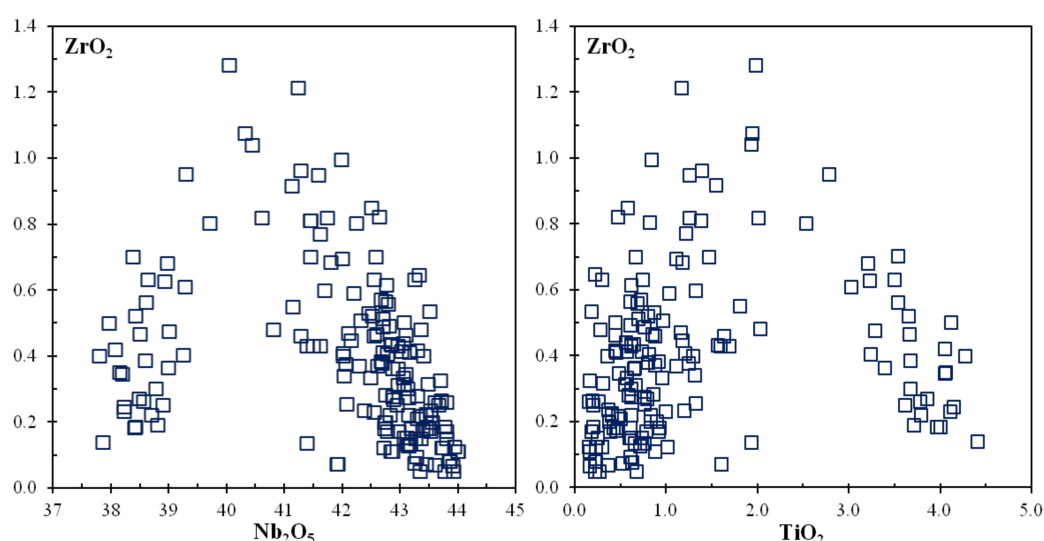


Figure 6. Variations of ZrO_2 versus Nb_2O_5 and TiO_2 in rippite (in wt %).

Table 2. Chemical composition (EMPA-WDS, wt %) of rippite from the Chuktukon calciocarbonatite (holotype sample 546-193.5), Chadobets upland, Siberia, Russia.

Component	1			2	3		4		5				6		7		8	9	
Grain				Nb3-1			Nb3-18			Nb3-13			Nb3-23		Nb4-28				
Position				c	or	c	m	r	or	or	c	r	c	r	c	r	inc	Ideal	
n	120	sd	Range	22	1	1	1	1	1	1	1	1	1	1	1	1	5		
SiO ₂	40.28	0.23	40.07–41.02	40.17	40.07	40.92	40.17	40.26	40.54	40.63	41.02	40.25	40.34	40.09	40.21	40.13	40.23	40.27	40.03
TiO ₂	1.11	1.06	0.15–4.41	0.52	0.15	4.05	0.58	1.18	2.01	3.02	4.41	0.45	1.39	0.26	0.74	0.57	0.82	0.91	0.00
ZrO ₂	0.37	0.26	0.05–1.28	0.17	0.26	0.35	0.85	0.68	0.82	0.61	0.14	0.42	0.96	0.26	0.63	0.33	0.80	0.26	
Nb ₂ O ₅	42.30	1.61	38.23–44.00	43.37	43.81	38.20	42.51	41.81	40.61	39.28	37.87	43.30	41.29	43.61	42.55	43.06	42.25	42.72	44.28
Na ₂ O	0.01	0.02	0.00–0.06	0.01	0.00	0.00	0.00	0.00	0.00	0.04	0.00	0.03	0.00	0.00	0.00	0.02	0.02	0.03	
K ₂ O	15.77	0.09	15.68–16.07	15.72	15.71	16.03	15.74	15.77	15.89	15.86	16.07	15.74	15.80	15.71	15.76	15.71	15.74	15.74	15.69
F	0.32	0.22	0.09–0.95	0.13	0.15	0.91	0.25	0.37	0.56	0.69	0.95	0.15	0.50	0.19	0.38	0.30	0.32	0.28	0.00
H ₂ O	0.18	0.05	0.12–0.26	0.18															
Sum	100.34			100.27	100.15	100.46	100.10	100.07	100.43	100.13	100.46	100.33	100.28	100.12	100.27	100.12	100.18	100.20	100.00
O-F ₂	0.14			0.05	0.06	0.38	0.11	0.16	0.24	0.29	0.40	0.06	0.21	0.08	0.16	0.13	0.13	0.12	0.00
Sum	100.20			100.22	100.09	100.07	99.99	99.92	100.19	99.84	100.06	100.27	100.07	100.04	100.11	99.99	99.99	100.08	100.00
Formula based on 8 cations																			
Si	4.000			4.000	3.999	3.999	4.001	4.001	4.000	4.001	4.001	4.000	4.000	4.001	4.000	4.000	4.000	4.001	4.000
Ti	0.083			0.039	0.011	0.298	0.043	0.088	0.149	0.224	0.324	0.033	0.104	0.019	0.055	0.042	0.061	0.068	0.000
Zr	0.018			0.008	0.013	0.016	0.041	0.033	0.039	0.029	0.007	0.020	0.047	0.013	0.031	0.016	0.039	0.012	
Nb	1.899			1.953	1.977	1.688	1.914	1.878	1.811	1.748	1.670	1.945	1.851	1.967	1.914	1.940	1.899	1.919	2.000
K + Na	2.000			2.000	2.000	2.000	2.000	1.999	2.000	2.000	1.999	2.001	1.999	2.000	2.000	2.001	2.000	2.000	2.000
F	0.101			0.041	0.049	0.281	0.079	0.116	0.175	0.215	0.293	0.046	0.157	0.060	0.120	0.095	0.101	0.088	0.000
OH	0.118			0.119															
End-members, mol. %																			
K ₂ Nb ₂ (Si ₄ O ₁₂)O ₂	0.95			0.98	0.99	0.84	0.96	0.94	0.91	0.87	0.83	0.97	0.93	0.98	0.96	0.97	0.95	0.96	1.00
K ₂ Ti ₂ (Si ₄ O ₁₂)(F,OH) ₂	0.05			0.02	0.01	0.16	0.04	0.06	0.09	0.13	0.17	0.03	0.07	0.02	0.04	0.03	0.05	0.04	0.00

Notes: *n*—number of analyses; Ta₂O₅, BaO, SrO, FeO, Al₂O₃, MgO, MnO and CaO are below detection limits (<0.005 wt %). 1—average composition of holotype rippite; 2—average composition for crystals used for SIMS (determination of H₂O and F); 3–7—individual crystals (see Figures 5, 8 and 12, Figures S6 and S7); 8 (inc)—from secondary inclusions in fluorcalciopyrochlore (Figure 4); 9—ideal composition K₂Nb₂(Si₄O₁₂)O₂; c, m, r and or—core, middle, rim and outermost rim of crystals.

Table 3. Representative compositions (EMPA-WDS, wt %) of rippite from other Chuktukon calciocarbonatites, Chadobets upland, Siberia, Russia.

Sample	514-231		514-231		549-192		549-192		549-192		549-192
Grain	R8-5		R8-4		R9-Rip2		R9-Rip3		R5-7		R5-3
Position	c	r	c	r	c	r	c	r	or	inc	inc
SiO ₂	40.20	40.30	40.31	40.43	40.19	40.44	40.10	40.35	41.04	40.17	40.75
TiO ₂	0.37	0.91	1.10	1.56	0.30	1.81	0.46	1.69	4.27	0.80	3.39
ZrO ₂	0.24	0.38	0.69	0.43	0.63	0.55	0.17	0.43	0.40	0.52	0.36
Nb ₂ O ₅	43.54	42.68	42.00	41.62	43.26	41.15	43.39	41.40	37.80	42.52	39.00
Na ₂ O	0.07	0.00	0.00	0.04	0.05	0.05	0.04	0.03	0.03	0.03	0.06
K ₂ O	15.64	15.81	15.80	15.78	15.67	15.76	15.67	15.78	16.04	15.71	15.89
F	0.11	0.12	0.50	0.29	0.23	0.51	0.34	0.57	0.74	0.55	0.84
Sum	100.17	100.20	100.41	100.15	100.33	100.27	100.17	100.25	100.31	100.31	100.29
O-F ₂	0.05	0.05	0.21	0.12	0.10	0.22	0.14	0.24	0.31	0.23	0.35
Sum	100.12	100.15	100.20	100.03	100.23	100.05	100.02	100.01	100.00	100.07	99.94
Formula based on 8 cations											
Si	4.002	3.998	4.000	4.001	4.001	4.000	4.000	3.999	4.001	4.000	4.000
Ti	0.027	0.068	0.082	0.116	0.022	0.134	0.034	0.126	0.313	0.060	0.250
Zr	0.011	0.019	0.034	0.021	0.031	0.027	0.008	0.021	0.019	0.025	0.017
Nb	1.959	1.914	1.884	1.862	1.947	1.840	1.957	1.855	1.666	1.914	1.731
K + Na	2.000	2.001	2.000	2.000	2.000	1.999	2.001	2.000	2.000	2.001	2.001
F	0.036	0.036	0.158	0.090	0.073	0.160	0.107	0.179	0.227	0.174	0.261
End-members, mol. %											
K ₂ Nb ₂ (Si ₄ O ₁₂)O ₂	0.98	0.96	0.94	0.93	0.97	0.92	0.98	0.93	0.83	0.96	0.87
K ₂ Ti ₂ (Si ₄ O ₁₂)(F,OH) ₂	0.02	0.04	0.06	0.07	0.03	0.08	0.02	0.07	0.17	0.04	0.13

Ta₂O₅, BaO, SrO, FeO, Al₂O₃, MgO, MnO and CaO are below detection limits (<0.005 wt %). c, m, r and or—core, middle, rim and outermost rim of crystals; inc—from secondary inclusions in fluorcalciopyrochlore. For samples: 514—number of drillhole; and 231—depths in drillhole. See Figure 4 and Figures S1–S4.

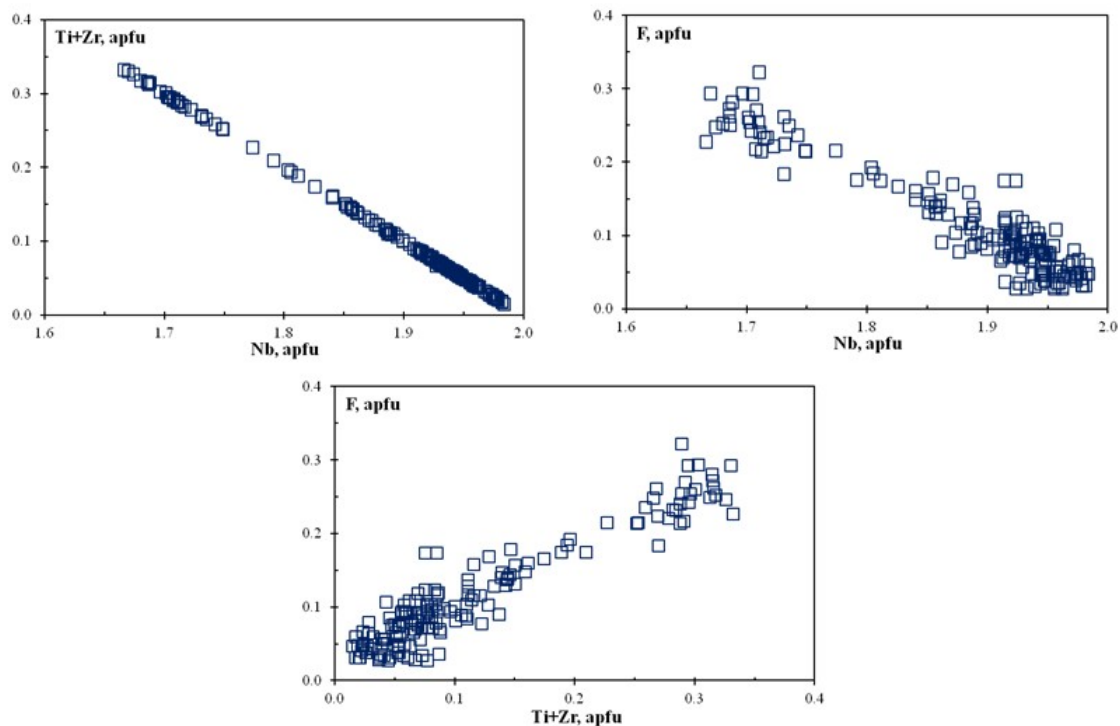
**Figure 7.** Compositional variations of rippite (in apfu).

Table 4. Major and trace element composition of individual grains of rippite from the Chuktukon calciocarbonatite (holotype sample 546-193.5), Chadobets upland, Siberia, Russia.

Component 1	2	3	4	5	6	7	8	9	10	
Grain	5-1Rp	5-2Rp	Rp-1	Rp-2	Rp-3	Rp-4	Rp-5	Rp-6-1	Rp-6-2	Rp-7
<i>n</i>	2	2	2	3	3	3	3	3	3	2
SiO ₂ , wt %	40.31	40.32	40.16	40.19	40.15	40.17	40.20	40.19	40.15	40.11
TiO ₂	0.65	0.83	0.87	0.62	0.44	0.45	0.49	0.69	0.39	0.23
ZrO ₂	0.21	0.32	0.20	0.22	0.18	0.30	0.15	0.17	0.05	0.08
Nb ₂ O ₅	42.88	43.22	42.75	43.17	43.48	43.37	43.48	43.1	43.69	43.87
Na ₂ O			0.00	0.04	0.00	0.03	0.00	0.00	0.02	0.00
K ₂ O	15.57	15.67	15.74	15.70	15.73	15.70	15.75	15.75	15.70	15.71
F			0.23	0.11	0.16	0.10	0.12	0.09	0.15	0.10
H ₂ O			0.16	0.17	0.25	0.17	0.14	0.13	0.26	0.12
Sum	99.61	100.34	100.10	100.21	100.39	100.29	100.33	100.12	100.40	100.21
O-F ₂			0.10	0.05	0.07	0.04	0.05	0.04	0.06	0.04
Sum	99.61	100.34	100.00	100.16	100.32	100.25	100.28	100.08	100.34	100.17
Li, ppm	0.36	0.37	0.22	0.31	0.11	0.05	0.11	0.13	1.23	0.03
Be			0.01	0.03	0.04	0.01	0.01	0.03	0.52	0.01
B			0.85	0.45	0.96	0.22	0.35	0.45	2.80	0.11
P	22	23								
Ca	16	16								
Ba	201	153								
Sr	1.31	0.70								
Sum	0.56	0.59								
REE	0.07	0.09								
Y	7.1	9.4								
Sc	1.61	0.56								
Ga	0.95	1.00								
Cr	26	12								
V	0.42	0.24								
Mn	0.03	0.03								
Co	0.25	0.26								
Ni	22	36								
Hf	7.3	11.3								
Ta	0.05	0.10								
Th	0.61	0.35								
U										

Notes: *n*—number of analyses; Al₂O₃, MgO, MnO and CaO are below detection limits (<0.005 wt %). 1–2—SEM-EDS + LA-ICP-MS [32]; 3–10 – SEM-EDS + SIMS (with determination of H₂O and F, author's data).

7. Optical Studies for Rippite

7.1. Cathodoluminescence

The CL images for single rippite crystals show green colour and very complex history during their growth (Figure 8). However, the individual zones and regions fixed in the CL images are weakly documented by the BSE images and elemental maps and do not reflect the variations in chemical composition (Figure 8, Figures S6 and S7). In general, the stages of nucleation, chaotic growth, dissolution and further growths may be observed in the CL images of individual rippite grains (Figure 8).

7.2. Transmission Spectra

The color of the powdered rippite is white and its crystals are almost colorless. Figure 9 shows the short-wave edge of the optical transmission spectra obtained for a crystal of about 150 × 150 mm² and about 100 mm thick, at 300 and 80 K. It is seen that the crystal becomes transparent from a wavelength of about 275 nm in the UV region of the spectrum. The Tauc analysis [51] indicates that

the spectra are straightened in coordinates $(\alpha^*(h\nu))^2 = f(h\nu)$, where α is the absorption coefficient and $h\nu$ is the photon energy. This is evidence that the shape of the fundamental absorption edge is determined by the direct allowed band-to-band electronic transitions. The position of the intersection points of straight lines with the abscissa axis determines the values of the band gap at 300 and 80 K: $E_g = 4.37$ and 4.50 eV, respectively. Under the action of laser radiation with a wavelength of 1052 nm, second-harmonic radiation (526 nm) is generated in the rippite powder. The intensity of the second harmonic is comparable to that obtained from the powder of the reference sample, a well-known nonlinear optical crystal, lithium iodate (LiIO_3), for which the second-order nonlinear susceptibility is $d_{31} = 4.1 \pm 0.4$ pm/V [52].

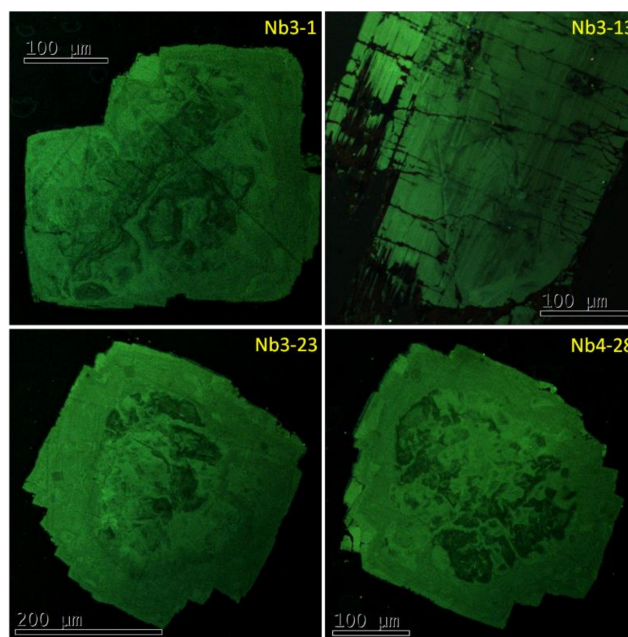


Figure 8. Cathodoluminescence images of rippite crystals.

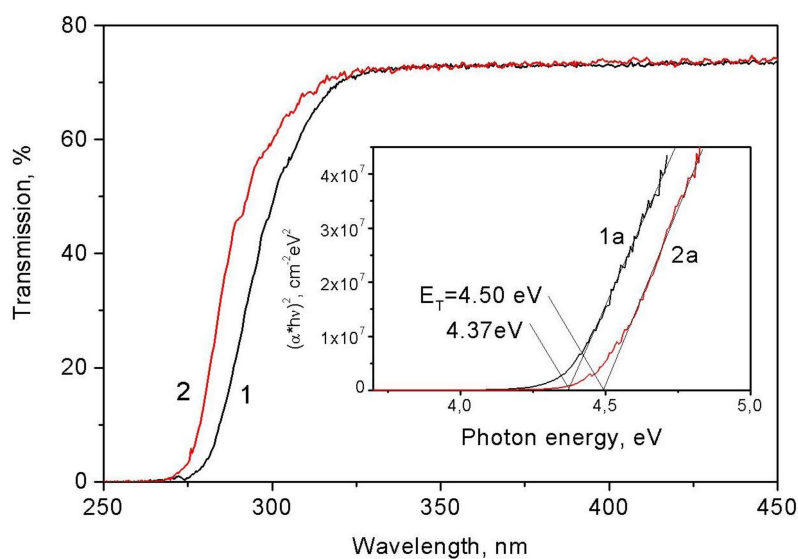


Figure 9. The short-wave edge of the rippite transmission spectra at 300 (curve 1) and 80 K (curve 2). In the insert: the Tauc plot for the case when the edge shape is determined by direct allowed electronic transitions. The band gap E_g for rippite is 4.37 and 4.50 eV at 300 and 80 K, respectively.

Rippite has a weak fluorescence and, in addition, its samples show spontaneous luminescence in the range of 100–400 K when heated or cooled at a rate of ~ 30 deg/min. This glow is typical for pyroelectrics [53] and indicates the absence of an inversion center in the structure. Indeed, rippite with a structure with a point group of $4mm$ belongs to one of the 10 crystallographic groups with a pyroelectric effect: $1, 2, 3, 4, 6, m, mm, mm2, 3m, 4mm$ and $6mm$ [54]. Such crystals have electric polarization even in the absence of an external electric field (spontaneous polarization). Pyroluminescence is the result of modifications in the atomic polarization in the crystal volume as temperature changes [53]. Flashes of light are the result of an electrical breakdown in pyroelectric fields, the intensity of which reaches hundreds of kV/cm.

7.3. Infrared and Raman Spectroscopy

Tetragonal rippite and its synthetic analog are related to space group $P4bm$ (No. 100), its point group is C_{4v} ($4mm$). Symmetry-representation analysis gives 105 modes of vibrations for rippite, which can be divided as $21A_1 + 16A_2 + 12B_1 + 17B_2 + 39E$, where $20A_1 + 38E$ vibrations are infrared active, $20A_1 + 12B_1 + 17B_2 + 38E$ vibrations are Raman active, and $16A_2$ vibrations are inactive in both regions. Acoustic modes $A_1 + E$ are not included here. Among these, the silicate tetrahedrons will share the following internal vibrations $5A_1 + 4B_1 + 5B_2 + 9E$. External vibrations include translation and SiO_4 libration modes. Their irreducible representations can be expressed as: $8A_1 + 7B_1 + 8B_2 + 18E$ and $7A_1 + B_1 + 4B_2 + 11E$, respectively. The C_{4v} point groups allow the simultaneous activity of some part of vibrations in both IR and Raman spectra [55]. The number of IR and Raman modes observed for rippite is far fewer than predicted, because of the low intensity of some modes and orientation effects. Crystals of Ti-poor rippite were mainly used for the IR and Raman spectroscopic studies.

7.3.1. Infrared Spectra

The following absorption bands are more remarkable in the IR spectra of rippite (in cm^{-1}): 395, 468, 493, 515, 553, 578, 686, 708, 784, 800, 818, 910, 967, 1087, 1166, 1245, 1388 and 1634 (powder KBr pellet, Figure 10). There are no clear bands in the $3000\text{--}4000\text{ cm}^{-1}$ region (Figures 10 and 11).

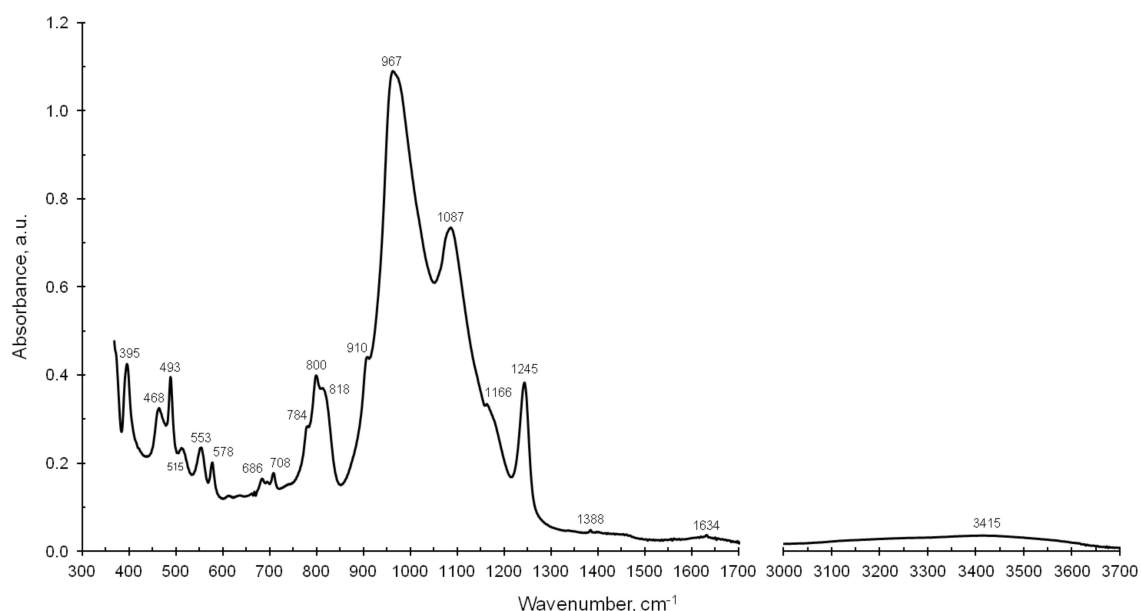


Figure 10. IR spectrum of rippite in the $350\text{--}1700$ and $3000\text{--}3700\text{ cm}^{-1}$ ranges (powder KBr pellet).

The strongest absorption band of the IR spectrum of rippite is 967 cm^{-1} (Figure 10) and assigned to be the ν_3 internal stretching mode of the SiO_4 tetrahedra. The antisymmetric stretching modes of the Si-O-Si bonds and the stretching vibrations of Si-O of the SiO_4 tetrahedra are active between 1300

and 960 cm^{-1} ; and symmetric stretching vibrational modes of the Si-O-Si bonds lying between 800 and 680 cm^{-1} . The latest bands are associated with the presence of bridging oxides (Si-O-Si linkage) in the structure. The stretching modes of the Nb-O bonds in the NbO_6 octahedra occur in the $600\text{--}800\text{ cm}^{-1}$ range as weak bands and shoulders, considering the stronger force constant of the Si-O bonds than that of the Nb-O ones. The bands below 580 cm^{-1} of the IR spectrum indicate silicon-oxygen bending vibrations and the stretching vibrations arising from K-O bonds. In addition, the IR and FTIR spectra of rippite show very weak and broad bands near 1634 and 3415 cm^{-1} (Figures 10 and 11). However, heating of rippite in powder KBr pellet up to 380°C and following IR measurements resulted to diminishing of these bands. Consequently, the presence of the substantial bands in the $1600\text{--}1700$ and $3400\text{--}3500\text{ cm}^{-1}$ region in unheated rippite samples may be partially related to absorbed H_2O . Nevertheless, we have to mention that our SIMS data indicate low H_2O content ($0.09\text{--}0.23\text{ wt \%}$) in the Ti-poor rippite. Thus, weak bands in the $3000\text{--}4000\text{ cm}^{-1}$ range, which may be related to the vibrations of (OH)-groups, unfortunately cannot outline the presence or absence of H_2O and as result the true H_2O concentration.

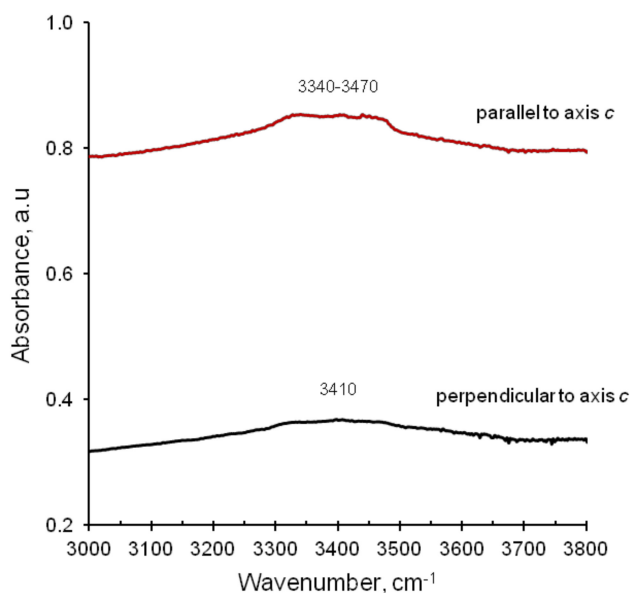


Figure 11. FTIR oriented spectra of rippite in the $3000\text{--}3800\text{ cm}^{-1}$ range (single crystal on KBr plate).

7.3.2. Raman Spectra

Main bands in oriented Raman spectra of rippite are (in cm^{-1}): 116, 144, 279, 324, 356, 397, 497, 652, 761, 807, 937, 1055 and 1112 (Figure 12). There are no clear bands in the $3000\text{--}4000\text{ cm}^{-1}$ region.

In general, bands below 360 cm^{-1} are ascribed to vibrations in polyhedra and octahedra as well as librational vibrations of the Si_4O_{12} group. Bands in the $390\text{--}700\text{ cm}^{-1}$ region are related to tetrahedral SiO_4 bending vibrations ($\nu_4 + \nu_2$). The strongest Raman band at 761 cm^{-1} (Figure 12) is assigned to be the internal stretching mode ν_1 of the SiO_4 tetrahedra. The ν_3 modes of the SiO_4 tetrahedra seem to be bands in the $900\text{--}1200\text{ cm}^{-1}$ region.

In addition, we tried to obtain data for rippite concerning to the dependence between chemical composition and changing in Raman spectra. For this purpose, we used zoned crystal Nb3-18. All spectra were obtained during one analytical session and in same conditions. The most substantial differences are visible for the bands at 934, 395 and 354 cm^{-1} (Figure 13). The increasing of the Ti(+Zr) content in rippite lead to left shifting for the 934 cm^{-1} band and to right shifting for the 395 and 354 cm^{-1} bands in Raman spectra. Unfortunately, such insufficient deviations (in $1\text{--}2\text{ cm}^{-1}$) cannot be used for identification of chemical composition for rippite according to Raman spectra.

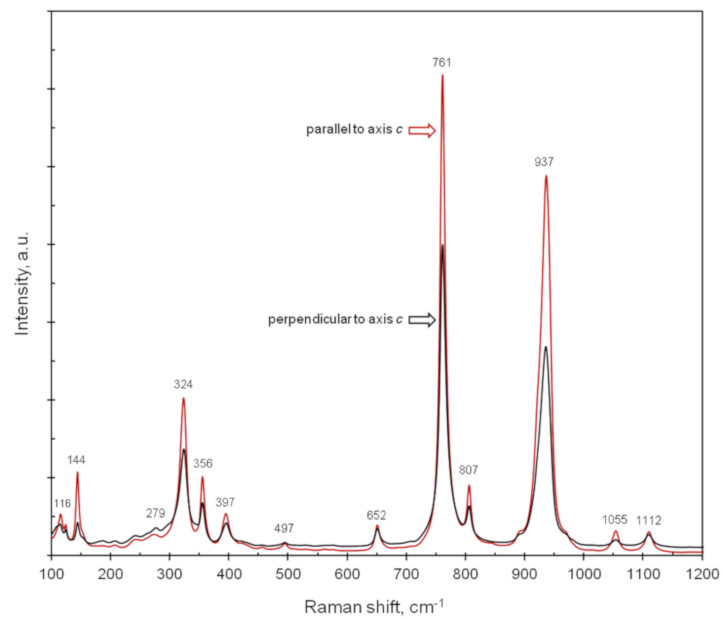


Figure 12. Oriented Raman spectra for single crystal of rippite.

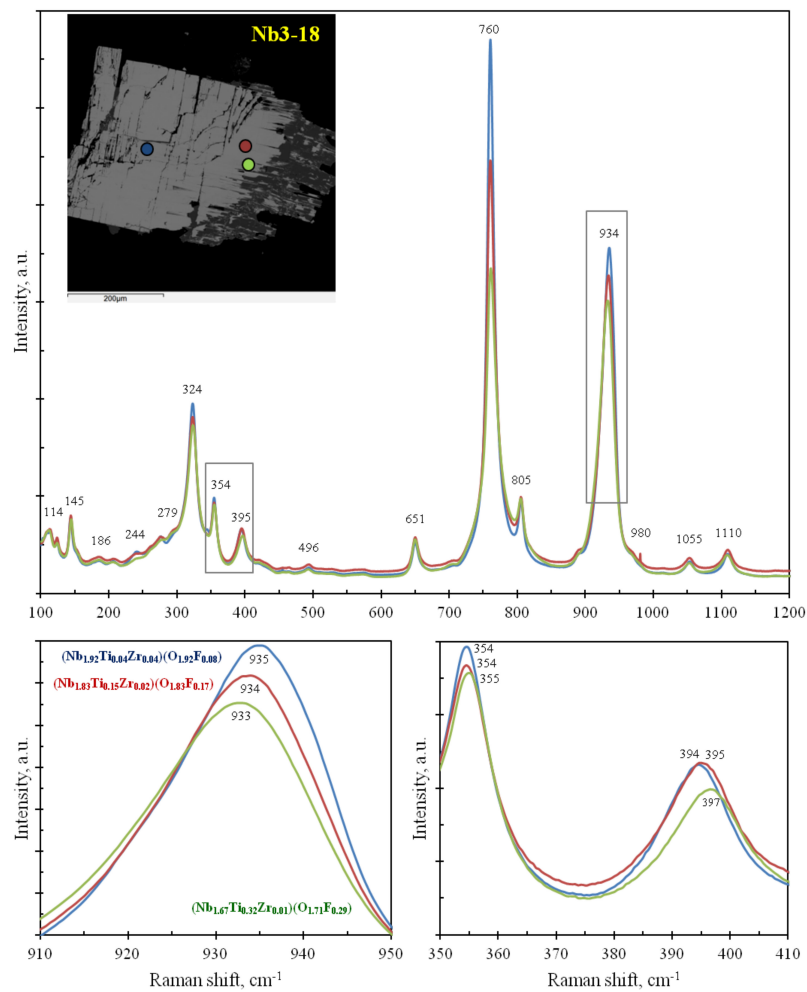


Figure 13. Raman spectra for a zoned rippite crystal showing dependence of some bands on chemical composition. For some details see Figures 5 and 8 and Table 2 and Table S1.

8. X-ray Crystallography and Crystal Structure of Rippite

The second harmonic generation test for rippite indicated the weak glow of powder, which was steady and green. The reference sample (LiIO_3), which is used in nonlinear optics, showed the same colour characteristics. All this strongly assumes a noncentro-symmetrical structure for rippite.

X-ray powder diffraction data for rippite (in Å for $\text{MoK}\alpha$) are given in Table 5. Unit cell parameters refined from the powder data using STOE Win XPOW 2.21 program package are as follows: tetragonal symmetry; space group $P4bm$; $a = 8.735(3)$ Å; $c = 8.127(5)$ Å; $V = 620.1(4)$ Å³; $Z = 2$.

Table 5. X-ray powder diffraction data for rippite ($\text{MoK}\alpha = 0.71073$ Å, Gandolfi geometry, $I > 1$).

<i>h</i>	<i>k</i>	<i>l</i>	<i>d</i> _{calc} (Å)	<i>d</i> _{obs} (Å)	<i>I</i>	<i>h</i>	<i>k</i>	<i>l</i>	<i>d</i> _{calc} (Å)	<i>d</i> _{obs} (Å)	<i>I</i>
0	0	1	8.127	8.161	4	1	5	0	1.713	1.712	19
1	1	0	6.177	6.205	100	2	2	4	1.697		
1	1	1	4.917	4.943	5	1	3	4	1.637	1.639	14
0	2	0	4.367	4.383	83	1	5	2	1.579	1.580	18
0	0	2	4.063	4.082	90	4	4	0	1.544	1.546	13
1	2	0	3.906	3.914	46	1	2	5	1.501	1.502	11
0	2	1	3.847	3.850	18	3	5	0	1.498		
1	2	1	3.521	3.530	87	0	4	4	1.487	1.491	7
1	1	2	3.395	3.405	40	1	4	4	1.466	1.469	5
2	2	0	3.088	3.096	59	0	6	0	1.456	1.460	5
0	2	2	2.975	2.985	81	4	4	2	1.443	1.446	8
1	2	2	2.816	2.822	70	2	4	4	1.408	1.410	11
1	3	0	2.762	2.768	99	2	6	0	1.381	1.383	6
2	2	2	2.459	2.466	7	2	3	5	1.350	1.351	3
2	3	0	2.423	2.426	3	1	5	4	1.310	1.309	16
2	3	1	2.322	2.324	6	2	6	2	1.308		
0	2	3	2.302	2.293	9	0	4	5	1.304		
1	3	2	2.284			3	6	0	1.302	1.301	11
0	4	0	2.184	2.187	3	0	2	6	1.294		
1	4	0	2.119	2.120	16	4	4	4	1.229	1.233	3
0	4	1	2.109			4	6	0	1.211	1.211	5
1	4	1	2.050	2.036	26	3	5	4	1.206		
0	0	4	2.032			2	7	0	1.200	1.206	5
2	4	0	1.953	1.955	44	0	6	4	1.183	1.184	3
1	3	3	1.934			4	6	2	1.161	1.161	2
1	1	4	1.930	1.930	23	3	7	0	1.147	1.148	6
0	4	2	1.924			2	6	4	1.142		
0	2	4	1.842	1.841	13	3	7	2	1.104	1.104	3
3	3	2	1.837			3	5	5	1.102		
2	3	3	1.806	1.810	5	3	6	4	1.096	1.098	2
2	4	2	1.760	1.762	25	0	8	2	1.054	1.058	3

The strongest diffraction lines are given in bold.

Single-crystal X-ray studies were carried out on a fragment of low-Ti rippite grain and gave the following results: tetragonal symmetry; space group $P4bm$; $a = 8.7388(2)$ Å; $c = 8.1277(2)$ Å; $V = 620.69(2)$ Å³; $Z = 2$. The crystal structure was studied for Ti-poor rippite $\text{K}_2(\text{Nb}_{1.93}\text{Ti}_{0.05}\text{Zr}_{0.02})[\text{Si}_4\text{O}_{12}]\text{O}(\text{O}_{0.93}\text{F}_{0.07})$. It was solved by direct methods and refined on the basis of 949 independent reflections (836 reflections with $I > 2\sigma(I)$). The factor R_1 for the crystal structure is 0.036. Crystallographic data for rippite are given in Tables 6–9. The crystal structure is shown in Figure 14. Rippite is closely identical in the crystal structure to synthetic compound $\text{K}_2\text{Nb}_2(\text{Si}_4\text{O}_{12})\text{O}_2$ (or KNbSi_2O_7) [3–5,15] (Figure 15).

The Nb^{5+} cations occupy two sites, which also contain minor amounts of Ti^{4+} and Zr^{4+} . The Nb sites are surrounded by six O atoms in octahedral coordination. The corner-shared NbO_6 octahedra form chains running parallel to a four-fold symmetry axes. The chains are coupled together by four-membered Si_4O_{12} rings so that each octahedron shares four corners with four SiO_4 tetrahedra belonging to four different Si_4O_{12} rings. Each Si_4O_{12} ring shares its terminal O atoms with eight NbO_6 octahedra of four neighboring chains linking them in the 3D heteropolyhedral framework.

The four-membered rings are in the plane {110}; at that each ring is connected with two neighboring Nb-octahedra of one chain via shared O-atoms forming heteropolyhedral four-membered rings (Figure 14b). Positions of K^+ are situated in channels which extend through the structure in the [001] direction. K^+ cations are coordinated by twenty O atoms in a form of a two-capped pentagonal prism. Low content of F does not give possibility to determine its structural position.

Table 6. Data collection and structure refinement details for rippite.

Crystal Data	
Unit cell dimensions (Å)	$a = 8.73885(16)$, $c = 8.1277(2)$
Space group	$P4bm$ (No. 100)
Volume (Å ³)	620.69(2)
Z	2
Chemical formula	$K_2(Nb_{1.93}Ti_{0.05}Zr_{0.02})(Si_4O_{12})O(O_{0.93}F_{0.07})$
Intensity Measurement	
Crystal shape	Fragment of prismatic crystal bounded by cleavage on (001)
Crystal size (mm)	$0.30 \times 0.24 \times 0.14$
Diffractometer	Oxford Diffraction Xcalibur Gemini
X-ray radiation	Mo K α
X-ray power	50 kV 30 mA
Monochromator	Graphite
Temperature	293 K
Detector to sample distance	85 mm
Measurement method	Omega scan
Radiation width	1°
Time per frame	5 s
Max. θ° -range for Data collection	32.04
Index ranges	$-6 \leq h \leq 12$ $-12 \leq k \leq 11$ $-11 \leq l \leq 9$
No. of measured reflections	3667
No. of unique reflections	949
No. of observed reflections ($I > 2\sigma(I)$)	834
Refinement of the structure	
No. of parameters used in refinement	63
R_{int}	0.0269
Flack x parameter	0.15(16)
R_1 , $I > 2\sigma(I)$	0.0360
R_1 all Data	0.0429
wR_2 on (F^2)	0.0980
GooF	1.109
$\Delta\rho$ min (e Å ⁻³)	−0.814 close to K1
$\Delta\rho$ max (e Å ⁻³)	0.855 close to Nb1

Table 7. Atom coordinates, U_{eq} (Å²) values, and occupancies for rippite.

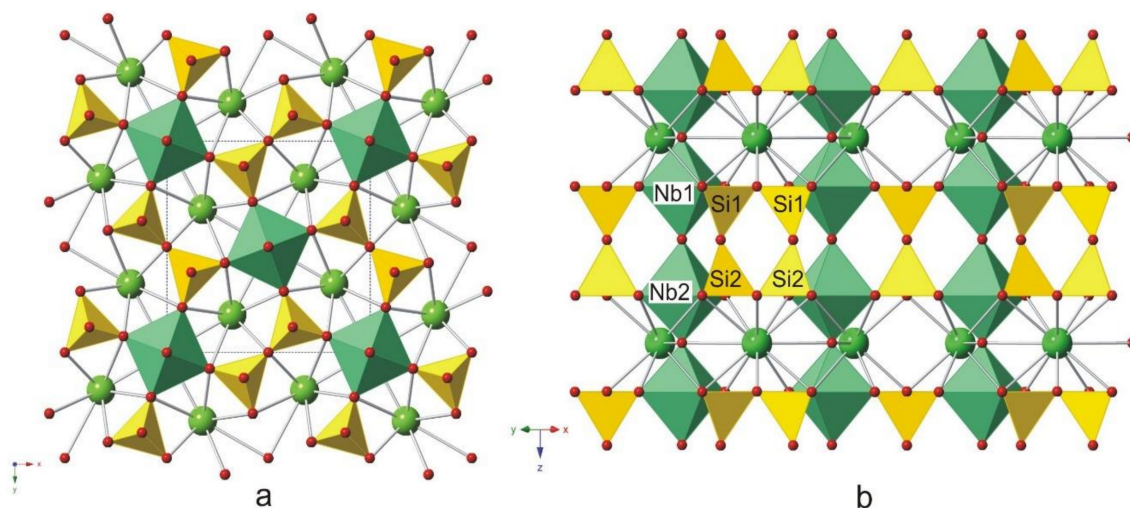
Atom	Occupancy	x	y	z	U_{eq}
Nb1	Nb _{0.96} Ti _{0.03} Zr _{0.01}	0.0	0.0	0.23217(13)	0.0255(2)
Nb2	Nb _{0.96} Ti _{0.03} Zr _{0.01}	0.0	0.0	0.73373(12)	0.0237(2)
K1	1	0.32254(8)	0.82254(8)	0.0003(3)	0.0216(2)
Si1	1	0.12425(14)	0.62425(14)	0.3080(2)	0.0139(3)
Si2	1	0.12401(13)	0.62401(13)	0.69906(18)	0.0076(3)
O1	1	0.4240(4)	0.2895(4)	0.2361(4)	0.0182(8)
O2	1	0.4229(5)	0.2877(5)	0.7680(3)	0.0158(9)
O3	1	0.0	0.0	−0.0020(14)	0.0200(11)
O4	1	0.0	0.0	0.4943(17)	0.0229(12)
O5	1	0.1204(3)	0.6204(3)	0.4974(8)	0.0203(7)
O6	1	0.5	0.0	0.2356(8)	0.0156(14)
O7	1	0.5	0.0	0.7679(7)	0.0138(17)

Table 8. Anisotropic displacement parameters (\AA^2) for rippite.

Atom	U^{11}	U^{22}	U^{33}	U^{12}	U^{13}	U^{23}
Nb1	0.0105(2)	0.0105(2)	0.0555(5)	0.0	0.0	0.0
Nb2	0.0114(2)	0.0114(2)	0.0483(5)	0.0	0.0	0.0
K1	0.0237(3)	0.0237(3)	0.0176(4)	−0.0041(3)	0.0004(6)	0.0004(6)
Si1	0.0141(5)	0.0141(5)	0.0133(7)	−0.0007(6)	−0.0001(4)	−0.0001(4)
Si2	0.0098(4)	0.0098(4)	0.0032(6)	0.0005(5)	−0.0002(4)	−0.0002(4)
O1	0.0189(16)	0.0109(14)	0.0247(15)	−0.0009(13)	−0.0029(12)	−0.0022(12)
O2	0.0217(19)	0.0147(18)	0.0110(14)	−0.0043(15)	−0.0001(11)	−0.0035(11)
O3	0.0161(12)	0.0161(12)	0.028(3)	0.0	0.0	0.0
O4	0.0194(13)	0.0194(13)	0.030(3)	0.0	0.0	0.0
O5	0.0264(9)	0.0264(9)	0.0080(14)	−0.0090(12)	−0.0054(18)	−0.0054(18)
O6	0.0139(18)	0.0139(18)	0.019(3)	0.005(3)	0.0	0.0
O7	0.017(2)	0.017(2)	0.007(3)	0.007(3)	0.0	0.0

Table 9. Bond lengths (\AA) for rippite.

Nb1–O3	1.903(12)	Nb2–O4	1.946(13)
Nb1–O1(4×)	1.956(4)	Nb2–O2(4×)	1.993(4)
Nb1–O4	2.131(13)	Nb2–O3	2.148(12)
mean	1.976	mean	2.011
K1–O2(2×)	2.874(4)	Si1–O5	1.541(7)
K1–O7	2.894(4)	Si1–O1(2×)	1.614(4)
K1–O1(2×)	2.898(4)	Si1–O6	1.644(3)
K1–O6	2.910(5)	mean	1.603
K1–O2(2×)	3.073(4)	Si2–O2(2×)	1.590(4)
K1–O1(2×)	3.088(4)	Si2–O7	1.632(2)
K1–O3(2×)	3.2171(3)	Si2–O5	1.639(7)
mean	3.009	mean	1.623

**Figure 14.** The crystal structure of rippite in (001) (a) and (110) (b) projections. Large green balls—K; small red balls—O.

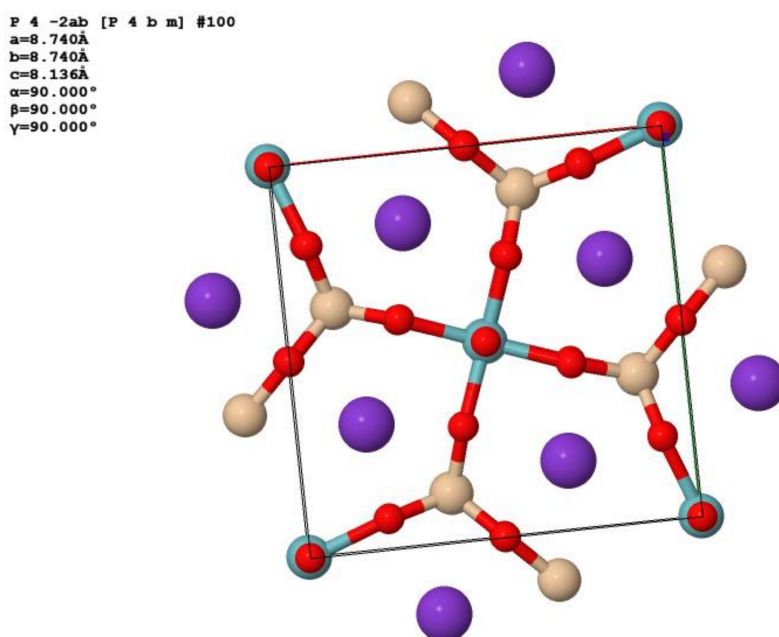


Figure 15. The crystal structure of the synthetic $K_2(NbO)_2Si_4O_{12}$ ($KNbSi_2O_7$) [15].

It should be noted that rippite is structurally related to cyclosilicates with $[Si_4O_{12}]^{8-}$ four-membered single rings. In structural and chemical aspects it seems to be in close with the labuntsovite-super group minerals, namely with vuoriyarvite-(K), $K_2(Nb,Ti)_2(Si_4O_{12})(O,OH)_2 \cdot 4H_2O$ (vuoriyarvite group, space group Cm , $a = 14.692 \text{ \AA}$, $b = 14.164 \text{ \AA}$, $c = 7.859 \text{ \AA}$, $Z = 4$; $\beta = 117.87^\circ$, $V = 1445.74 \text{ \AA}^3$) [56–60]. However, rippite is nominally free in H_2O and (OH) -groups. In addition, the connection of the octahedral chains and $[Si_4O_{12}]$ -rings is quite different in the crystal structure of rippite (this work) and the labuntsovite-super group minerals [56–60]. Unlike rippite the four-membered tetrahedral rings in the structure of vuoriyarvite-(K) are oriented perpendicularly to the NbO_6 -chains and two neighboring Nb-octahedra in one chain are connected by shared O-atoms with edge of the SiO_4 -tetrahedron. It led to considerable deformation of the octahedral chain. In general, we suggest that the rippite-related structure is a new structural type among cyclosilicates with the $[Si_4O_{12}]^{8-}$ single rings.

The compound $K_4(NbO)_2[Si_8O_{21}]$ is somewhat close in element suite, chemistry and structure to rippite and synthetic $K_2(NbO)_2Si_4O_{12}$ [61,62]. It was synthesized in the hydrothermal system $K_2O-Nb_2O_5-SiO_2-H_2O$ ($T = 450\text{--}500^\circ\text{C}$; $P = 1000\text{--}1200 \text{ bar}$) and its composition is (EMPA, in wt %): SiO_2 —51.10; Nb_2O_5 —28.80; K_2O —20.84 [61]. Unlike rippite and its synthetic analog this phase has complex modulated structure and triclinic symmetry: space group $P-1$; $a = 33.92(2) \text{ \AA}$, $b = 10.950(6) \text{ \AA}$, $c = 7.737(4) \text{ \AA}$, $\alpha = 76.42(4)^\circ$, $\beta = 72.10(5)^\circ$, $\gamma = 89.81(5)^\circ$, $V = 2650.8 \text{ \AA}^3$ [62]. In addition, $K_4(NbO)_2[Si_8O_{21}]$ is characterized by a relatively low nonlinear polarization in comparison with $K_2(NbO)_2Si_4O_{12}$ owing to the low concentration of the isolated NbO_6 octahedra in its structure [63]. In contrast with this K-Nb-silicate, rippite and synthetic $K_2(NbO)_2Si_4O_{12}$ display a strong non-linear effect, as the NbO_6 octahedra are linked in columns (Figures 14 and 15).

9. Discussion and Concluding Remarks

In general the detailed studies for the Chuktukon calciocarbonatites (Chadobets upland, Krasnoyarsk Territory, Russia) gave the possibility of describing the chemical composition and crystal structure for a new mineral, rippite $K_2(Nb,Ti)_2(Si_4O_{12})(O,F)_2$, which belongs to a new structural type among the $[Si_4O_{12}]$ -cyclosilicates and is close to the labuntsovite super group. This mineral is related to primary phases, which were crystallized after fluorcalciopyrochlore, the main carrier of Nb in the calciocarbonatites. The primary carbonatite paragenesis may be formed at temperatures

near and below 837 °C according to the calcite-dolomite thermometer. The synthesis in the system $\text{SiO}_2\text{-Nb}_2\text{O}_5\text{-K}_2\text{O}$ has indicated that the $\text{K}_2\text{Nb}_2(\text{Si}_4\text{O}_{12})\text{O}_2$ phase may be stable in the 510–735 °C temperature range [4,6,8–10,13,14].

Rippite is the second main mineral to concentrate Nb in the Chuktukon calciocarbonatites [1,2,29,32]. The presence of this mineral should be into account in processing schemes of carbonatitic Nb-ores, as in some rock species the modal contents of pyrochlore and rippite may be equal. The weathered carbonatites are the basis of the Chuktukon niobium-rare earth elements ore deposit, which is very promising for development in eastern Siberia in a future [40–42]. It is quite possible that unweathered calciocarbonatites will be also involved in processing schemes. In general, it is concerning not only to the Chuktukon calciocarbonatites, but and to other pyrochlore-rich carbonatites around the world [64]. At present rippite was found only in calciocarbonatites of the Chuktukon massif. However, we are not sure that this mineral is endemic for the Chuktukon rocks and may be also occur in other pyrochlore-containing carbonatites worldwide.

It should be noted that the mineral phase with ratio of the main components (K:Nb:Si) similar to rippite has been described as minute inclusions in late apatite aggregates from calciocarbonatites of the Araxá alkaline-carbonatite complex, Brazil [65]. According to chemistry (SiO_2 —37.9–39.3 wt %; Nb_2O_5 —34.7–37.6 wt %; TiO_2 —0.3–1.6 wt %; K_2O —14.2–14.4 wt %) and low total sums this mineral was identified as nenadkevichite (labuntsovite supergroup). Probably further studies will clearly outline whether the Araxá mineral is rippite or it is vuoriyarvite-K (labuntsovite supergroup).

The discovery of rippite also highlights some problems in the synthesis and growth of high-quality crystals suitable for industrial purposes. It is known that synthetic analog of rippite is a good material for nonlinear optics [3–14]. Ideal and large single crystals of KNbSi_2O_7 (near 1 cm) of high optical quality, which are valid for industrial purpose, are still rarity [14]. The mineral association of rippite-containing calciocarbonatites may be a key in understanding of favorable conditions for synthesis of the perfect KNbSi_2O_7 crystals (Ca-rich carbonate environment).

The compositional study of rippite strongly suggests the incorporation of (Ti,Zr) and F in the structure via the isomorphism $\text{Nb}^{5+} + \text{O}^{2-} \rightarrow (\text{Ti,Zr})^{4+} + \text{F}^{1-}$. As a result the content of a hypothetical end-member $\text{K}_2\text{Ti}_2[\text{Si}_4\text{O}_{12}]\text{F}_2$ in rippite may be up to 17 mol. %. Unfortunately, there are no any data about synthesis of $\text{K}_2\text{Ti}_2[\text{Si}_4\text{O}_{12}]\text{F}_2$ or $\text{K}_2\text{Zr}_2[\text{Si}_4\text{O}_{12}]\text{F}_2$, which may be isostructural with $\text{K}_2\text{Nb}_2(\text{Si}_4\text{O}_{12})\text{O}_2$ and $\text{K}_2\text{Ta}_2(\text{Si}_4\text{O}_{12})\text{O}_2$ [3–5,16]. It is quite possible that Ti- and Zr-counterparts or their intermediate compositions with $\text{K}_2\text{Nb}_2(\text{Si}_4\text{O}_{12})\text{O}_2$ will have higher nonlinearity rather than pure $\text{K}_2\text{Nb}_2(\text{Si}_4\text{O}_{12})\text{O}_2$. From other side the minimal doping of the $\text{K}_2\text{Nb}_2(\text{Si}_4\text{O}_{12})\text{O}_2$ compound by Ti or Zr may lead to good conditions for single crystal fabrication.

It should be also mentioned that rippite has been successfully used as a geochronometer. The Ar-Ar age estimated for rippite from the Chuktukon calciocarbonatite (sample 546-193.5) is 231.1 ± 2.7 Ma [31].

Supplementary Materials: The following figures are available online at <http://www.mdpi.com/2075-163X/10/12/1102/s1>: Figure S1: Secondary polymineral inclusions with rippite in fluorcalciopyrochlore, Chuktukon calciocarbonatite, BSE images and elemental maps; Figure S2: Inclusions of fluorcalciopyrochlore in rippite, Chuktukon calciocarbonatite, BSE images and elemental maps; Figure S3: Relationship of rippite with tainiolite in the Chuktukon calciocarbonatite, BSE images and elemental maps; Figure S4: The outer zone in a rippite crystal and its replacement by quartz with formation of the TiO_2 phase (rutile ?), Chuktukon calciocarbonatite, BSE image and elemental maps; Figure S5: Replacement of rippite by quartz with formation of the TiO_2 phase (rutile ?), Chuktukon calciocarbonatite, BSE images and elemental maps; Figure S6: BSE and CL images and elemental maps for low-Ti rippite (grain Nb3-1), Chuktukon calciocarbonatite; Figure S7: BSE and CL images and elemental maps for low-Ti rippite (grain Nb3-23), Chuktukon calciocarbonatite. Supplementary materials also include Table S1: Chemical composition (WDS, wt %) of rippite from the Chuktukon calciocarbonatite, Chadobets upland, Siberia, Russia and CIF file for rippite.

Author Contributions: V.V.S. and A.G.D wrote the paper and performed the mineralogical description for carbonatites; the crystal structure and X-ray powder data for rippite, Y.V.S.; optical and physical properties for rippite, E.V.B.; Raman spectroscopy and SIMS, V.V.S.; SEM and CL, V.V.S., N.S.K. and A.G.D.; EMPA, V.V.S. and E.N.N.; LA ICP-MS—A.G.D.; IR spectroscopy, T.N.M. and I.N.K., second harmonic generation test, A.P.Y. and V.N.V. All authors have read and agreed to the published version of the manuscript.

Funding: Investigations of inclusions in minerals and physical and chemical properties of rippite were done on state assignment of IGM SB RAS (0330-2019-0002 and 0330-2016-0005) and GIN SB RAS (AAAA-A16-116122110027-2), and the Initiative Project of Ministry of Science and Higher Education of the Russian Federation, Act 211 of the Government of the Russian Federation (agreement no. 02.A03.21.0006). Geochemical, spectroscopic and chemical studies for rippite were supported by the Russian Science Foundation (grant 19-17-00019).

Acknowledgments: The author would like to thank M.V. Khlestov (IGM, Novosibirsk, Russia), S.G. Simakin and Ye.V. Potapov (YBPTI, Yaroslavl, Russia) and H. Bratz (Erlangen, Germany) for their technical assistance during SEM, SIMS and LA-ICP-MS studies. We are highly appreciative of the comments and suggestions of four anonymous reviewers.

Conflicts of Interest: The authors declare no conflict of interest.

References

- Doroshkevich, A.G.; Sharygin, V.V.; Seryotkin, Y.V.; Karmanov, N.S.; Belogub, E.V.; Moroz, T.N.; Nigmatulina, E.N.; Eliseev, A.P.; Vedenyapin, V.N.; Kupriyanov, I.N. Rippite, IMA 2016-025. CNMNC Newsletter no. 32, August 2016, page 919. *Mineral. Mag.* **2016**, *80*, 915–922.
- Sharygin, V.V.; Doroshkevich, A.G.; Seryotkin, Y.V.; Karmanov, N.S.; Belogub, E.V.; Moroz, T.N. A new K-Nb-cyclosilicate $K_2(Nb,Ti)_2(Si_4O_{12})O(O,F)$ from Chuktukon carbonatite massif, Chadobets upland, Russia. In Proceedings of the Abstract Volume of Second European Mineralogical Conference, Rimini, Italy, 11–15 September 2016; p. 421.
- Crosnier, M.P.; Guyomard, D.; Verbaere, A.; Piffard, Y.; Tournoux, M. $K_2(NbO)_2Si_4O_{12}$: A new material for non-linear optics. *Ferroelectrics* **1991**, *124*, 61–66. [[CrossRef](#)]
- Foster, M.C.; Arbogast, D.J.; Photinos, P.; Nielson, R.M.; Abrahams, S.C. $K_2(NbO)_2Si_4O_{12}$: A new ferroelectric. *J. Appl. Crystallogr.* **1999**, *32*, 421–425. [[CrossRef](#)]
- Crosnier, M.P.; Guyomard, D.; Verbaere, A.; Piffard, Y.; Tournoux, M. The potassium niobyl cyclotetrasilicate $K_2(NbO)_2Si_4O_{12}$. *J. Solid State Chem.* **1992**, *98*, 128–132. [[CrossRef](#)]
- Tanaka, H.; Yamamoto, M.; Takahashi, Y.; Benino, Y.; Fujiwara, T.; Komatsu, T. Crystalline phases and second harmonic intensities in potassium niobium silicate crystallized glasses. *Opt. Mater.* **2003**, *22*, 71–79. [[CrossRef](#)]
- Pernice, P.; Aronne, A.; Sigaev, V.N.; Sarkisov, P.D.; Molev, V.I.; Stefanovich, S.Y. Crystallization behavior of potassium niobium silicate glasses. *J. Am. Ceram. Soc.* **1999**, *82*, 3447–3452. [[CrossRef](#)]
- Sigaev, V.N.; Lotarev, S.V.; Ryzhenkov, V.S.; Golubev, N.V.; Stefanovich, S.Y.; Champagnon, B.; Vouagner, D.; Nardou, E.; Porcar, L.; Paleari, A.; et al. Nano-heterogeneous structure of $(1-x)KNbO_3-xSiO_2$ glasses in the low glass-forming oxide content range $0.05 \leq x \leq 0.3$. *J. Non-Cryst. Solids* **2011**, *357*, 3136–3142. [[CrossRef](#)]
- Sigaev, V.N.; Ryzhenkov, V.S.; Lotarev, S.V.; Golubev, N.V.; Stefanovich, S.Y.; Okada, A. Glasses and their crystallization in the $(1-x)KNbO_3-xSiO_2$ system at low glass-forming oxide contents, $0 \leq x \leq 0.35$. *J. Non-Cryst. Solids* **2010**, *356*, 958–965. [[CrossRef](#)]
- Sigaev, V.N.; Stefanovich, S.Y.; Champagnon, B.; Gregora, I.; Pernice, P.; Aronne, A.; LeParc, R.; Sarkisov, P.D.; Dewhurst, C. Amorphous nanostructuring in potassium niobium silicate glasses by SANS and SHG: A new mechanism for second-order optical non-linearity of glasses. *J. Non-Cryst. Solids* **2002**, *306*, 238–248. [[CrossRef](#)]
- Aronne, A.; Sigaev, V.N.; Pernice, P.; Fanelli, E.; Usmanova, L.Z. Non-isothermal crystallization and nanostructuring in potassium niobium silicate glasses. *J. Non-Cryst. Solids* **2004**, *337*, 121–129. [[CrossRef](#)]
- Santos, R.; Santos, L.F.; Almeida, R.M.; Deubener, J.; Wondraczek, L. Crystallization of niobium germanosilicate glasses. *J. Solid State Chem.* **2010**, *183*, 128–135. [[CrossRef](#)]
- Vernacotola, D.E.; Shelby, J.E. Potassium niobium silicate glasses. *Phys. Chem. Glasses* **1994**, *35*, 153–159.
- Sahashi, A.; Hoshina, T.; Takeda, H.; Tsurumi, T. Fabrication of ferroelectric silicate $KNbSi_2O_7$ single crystal. *J. Ceram. Soc. Jpn.* **2014**, *122*, 389–392. [[CrossRef](#)]
- Gopalakrishnan, J.; Ramesha, K.; Rangan, K.K.; Pandey, S. In Search of Inorganic Nonlinear Optical Materials for Second Harmonic Generation. *J. Solid State Chem.* **1999**, *148*, 75–80. [[CrossRef](#)]
- Lee, J.-G.; Höhn, P.; Greenblatt, M. A potassium tantalum (V) tetrasilicate $KTaSi_2O_7$. *J. Solid State Chem.* **1996**, *123*, 123–128. [[CrossRef](#)]
- Ripp, G.S.; Khodanovich, P.Y.; Smirnova, O.K. New data on the carbonatite nature of the Khalyuta deposit. *Dokl. Earth Sci.* **1999**, *365*, 351–353.

18. Ripp, G.S.; Khodanovich, P.Y.; Smirnova, O.K. A new carbonatite province in West Transbaikalia. *Geologiya i Geofizika* **1999**, *40*, 73–81.
19. Ripp, G.S.; Badmatsyrenov, M.V.; Skulyberdin, A.A. A new carbonatite occurrence in Northern Transbaikalia. *Petrology* **2002**, *10*, 391–394.
20. Ripp, G.S.; Badmatsyrenov, M.V.; Doroshkevich, A.G.; Izbrodin, I.A. New carbonatite-bearing area in northern Transbaikalia. *Petrology* **2005**, *13*, 489–498.
21. Ripp, G.S.; Doroshkevich, A.G.; Karmanov, N.S.; Kanakin, S.V. Micas from the Khaluta carbonatite deposit, western Transbaikalia region. *Geol. Ore Depos.* **2009**, *51*, 812–821. [[CrossRef](#)]
22. Ripp, G.S.; Doroshkevich, A.G.; Posokhov, V.F. Age of carbonatite magmatism in Transbaikalia. *Petrology* **2009**, *17*, 73–89. [[CrossRef](#)]
23. Ripp, G.S.; Doroshkevich, A.G.; Posokhov, V.F.; Izbrodin, I.A.; Konopel'ko, D.L.; Sergeev, S.A. The age of carbonatites and mafic rocks (SHRIMP II and Rb-Sr dating) from the Oshurkovo apatite-bearing pluton (western Transbaikalia). *Russ. Geol. Geophys.* **2011**, *52*, 517–525. [[CrossRef](#)]
24. Doroshkevich, A.G.; Ripp, G.S. Estimation of the conditions of formation of REE-carbonatites in western Transbaikalia. *Geologiya i Geofizika* **2004**, *45*, 492–500.
25. Doroshkevich, A.G.; Wall, F.; Ripp, G.S. Calcite-bearing dolomite carbonatite dykes from Veseloe, North Transbaikalia, Russia and possible Cr-rich mantle xenoliths. *Mineral. Petrol.* **2007**, *90*, 19–49. [[CrossRef](#)]
26. Doroshkevich, A.G.; Wall, F.; Ripp, G.S. Magmatic graphite in dolomite carbonatite at Pogranichnoe, North Transbaikalia, Russia. *Contrib. Mineral. Petrol.* **2007**, *153*, 339–353. [[CrossRef](#)]
27. Doroshkevich, A.G.; Ripp, G.S.; Viladkar, S.G.; Vladyskin, N.V. The Arshan REE carbonatites, southwestern Transbaikalia, Russia: Mineralogy, paragenesis and evolution. *Can. Mineral.* **2008**, *46*, 807–823. [[CrossRef](#)]
28. Doroshkevich, A.G.; Ripp, G.S.; Moore, K.R. Genesis of the Khaluta alkaline-basic Ba-Sr carbonatite complex (West Transbaikalia, Russia). *Mineral. Petrol.* **2010**, *98*, 245–268. [[CrossRef](#)]
29. Doroshkevich, A.G.; Chebotarev, D.A.; Sharygin, V.V.; Prokopyev, I.R.; Nikolenko, A.M. Petrology of alkaline silicate rocks and carbonatites of the Chuktukon massif, Chadobets upland, Russia: Sources, evolution and relation to the Triassic Siberian LIP. *Lithos* **2019**, *332–333*, 245–260. [[CrossRef](#)]
30. Doroshkevich, A.G.; Sharygin, V.V.; Belousova, E.A.; Izbrodin, I.A.; Prokopyev, I.R. Zircon from the Chuktukon alkaline ultramafic carbonatite complex (Chadobets uplift, Siberian craton) as evidence of source heterogeneity. *Lithos* **2020**. submitted.
31. Chebotarev, D.A.; Doroshkevich, A.G.; Sharygin, V.V.; Yudin, D.S.; Ponomarchuk, A.V.; Sergeev, S.A. Geochronology of the Chuktukon carbonatite massif, Chadobets uplift (Krasnoyarsk Territory). *Russ. Geol. Geophys.* **2017**, *58*, 1222–1231. [[CrossRef](#)]
32. Chebotarev, D.A.; Doroshkevich, A.G.; Klemd, R.; Karmanov, N.S. Evolution of Nb-mineralization in the Chuktukon carbonatite massif, Chadobets upland (Krasnoyarsk Territory, Russia). *Periodico di Mineralogia* **2017**, *86*, 99–118. [[CrossRef](#)]
33. Sharygin, V.V. Tainiolite from Chuktukon Carbonatite Massif, Chadobets Upland, Russia. In Proceedings of the Abstract Volume of XXXIV International Conference “Magmatism of the Earth and Related Strategic Metal Deposits”, Miass, Russia, 4–9 August 2017; pp. 242–244.
34. Sharygin, V.V.; Doroshkevich, A.G. Multiphase inclusions in zircons from Chuktukon carbonatite massif, Chadobets upland, Russia. In Proceedings of the Abstract Volume of XXXIV International Conference “Magmatism of the Earth and Related Strategic Metal Deposits”, Miass, Russia, 4–9 August 2017; pp. 244–247.
35. Sharygin, V.V.; Doroshkevich, A.G.; Chebotarev, D.A. Na-Sr-Ba-REE-carbonates and phosphates in minerals of Chuktukon massif carbonatites, Chadobets upland, Krasnoyarsk territory. In Proceedings of the Abstract Volume of XVII Russian Fluid Inclusion Conference, Ulan-Ude, Russia, 12–17 September 2016; pp. 180–182. (In Russian).
36. Kirichenko, V.T.; Zuev, V.K.; Perfilova, O.Y.; Sosnovskaya, O.V.; Smokotina, I.; Markovich, L.A.; Borodin, M.E.; Mironyuk, E. *State Geological Map of Russian Federation, Scale 1:1000000 (Third Generation)*; Ser. Angaro-Yeniseysk. Sheet O-47 Bratsk. Explanatory Note; Cartografic Factory of VSEGEI: St. Petersburg, Russia, 2012; pp. 163–179. (In Russian)
37. Dashkevich, N.N. Regional prediction of kimberlite magmatism in the southwestern Siberian Platform. In *Geology and Mineral Resources of Krasnoyarsk Territory*; Krasnoyarsk, Russia, 1999; pp. 31–42. (In Russian)

38. Starosel'tsev, V.S. Identifying paleorifts as promising tectonic elements for active oil and gas generation. *Russ. Geol. Geophys.* **2009**, *50*, 358–364. [\[CrossRef\]](#)
39. Prokopyev, I.; Starikova, A.; Doroshkevich, A.; Nugumanova, Y.; Potapov, V. Petrogenesis of ultramafic lamprophyres from the Terina complex (Chadobets upland, Russia): Mineralogy and melt inclusion composition. *Minerals* **2020**, *10*, 419. [\[CrossRef\]](#)
40. Tsikyna, S.V. The Nb-REE Chuktukon Deposit: Modelling, Ore Typification and Assessment of Prospects. Ph.D. Thesis, The Krasnoyarsk Research Institute of Geology and Mineral Resources, Krasnoyarsk, Russia, 2004. (In Russian).
41. Lomayev, V.G.; Serdyuk, S.S. The Chuktukon Nb-REE deposit—The priority object for modernization of the Russian rare-earth industry. *J. Sib. Fed. Univ. Eng. Technol.* **2011**, *4*, 132–154. (In Russian)
42. Serdyuk, S.S.; Lomayev, V.G.; Kuzmin, V.I.; Flett, D.S.; Gudkova, N.V.; Kuzmin, D.V.; Mulagaleeva, M.A.; Kuzmina, V.N.; Kalyakin, S.N.; Logutenko, O.A. The Chuktukon niobium-rare earth metals deposit: Geology and investigation into the processing options of the ores. *Miner. Eng.* **2017**, *113*, 8–14. [\[CrossRef\]](#)
43. Nosova, A.A.; Kargin, A.V.; Sazonova, L.V.; Dubinina, E.O.; Chugaev, A.V.; Lebedeva, N.M.; Yudin, D.S.; Larionova, Y.O.; Abersteiner, A.; Gareev, B.I.; et al. Sr-Nd-Pb isotopic systematic and geochronology of ultramafic alkaline magmatism of the southwestern margin of the Siberian Craton: Metasomatism of the sub-continental lithospheric mantle related to subduction and plume events. *Lithos* **2020**, *364*, 105509. [\[CrossRef\]](#)
44. Kargin, A.V.; Nosova, A.A.; Postnikov, A.V.; Chugaev, A.V.; Postnikova, O.V.; Popova, L.P.; Poshibaev, V.V.; Sazonova, L.V.; Dokuchaev, A.Y.; Smirnova, M.D. Devonian ultramafic lamprophyre in the Irkineeva–Chadobets trough in the southwest of the Siberian Platform: Age, composition, and implications for diamond potential prediction. *Geol. Ore Depos.* **2016**, *58*, 383–403. [\[CrossRef\]](#)
45. Nosova, A.A.; Sazonova, L.V.; Kargin, A.V.; Smirnova, M.D.; Lapin, A.V.; Shcherbakov, V.D. Olivine in ultramafic lamprophyres: Chemistry, crystallisation, and melt sources of Siberian pre- and post-trap aillikites. *Contrib. Mineral. Petrol.* **2018**, *173*, 55. [\[CrossRef\]](#)
46. Lapin, A.V. About kimberlites of the Chadobets upland in connection with a problem of the formational-metallogeny analysis of the platform alkaline ultrabasic magmatic rocks. *Otechestvennaya Geol.* **2001**, *4*, 30–35. (In Russian)
47. Lapin, A.V.; Lisitsyn, D.V. About mineralogical typomorphism of alkaline ultrabasic magmatic rocks of Chadobets upland. *Otechestvennaya Geol.* **2004**, *6*, 83–92. (In Russian)
48. Jochum, K.P.; Dingwell, D.B.; Rocholl, A.; Stoll, B.; Hofmann, A.W.; Becker, S.; Besmehn, A.; Bessette, D.; Dietze, H.-J.; Dulski, P.; et al. The preparation and preliminary characterisation of eight geological MPI-DING reference glasses for in-situ microanalysis. *Geostand. Newsl. J. Geostand. Geoanal.* **2000**, *24*, 87–133. [\[CrossRef\]](#)
49. Pearce, N.J.G.; Perkins, W.T.; Westgate, J.A.; Gorton, M.P.; Jackson, S.E.; Neal, C.R.; Chenery, S.P. A compilation of new and published major and trace element data for NIST SRM 610 and NIST SRM 612 glass reference materials. *Geostand. Newsl. J. Geostand. Geoanal.* **1997**, *21*, 115–144. [\[CrossRef\]](#)
50. Van Achterbergh, E.; Ryan, C.G.; Jackson, S.E.; Griffin, W.L. Data reduction software for LA-ICP-MS: Appendix. In *Laser Ablation-ICP-mass Spectrometry in the Earth Sciences: Principles and Applications*; MAC Short Course Series; Sylvester, P.J., Ed.; Mineralog. Assoc. Canada (MAC): Ottawa, ON, Canada, 2001; Volume 29, pp. 239–243.
51. Tauc, J. Optical properties and electronic structure of amorphous Ge and Si. *Mater. Res. Bull.* **1967**, *3*, 37–46. [\[CrossRef\]](#)
52. Nikogosyan, D. Nonlinear optical crystals. In *Complete Survey*; Springer Science + Business Media Inc.: New York, NY, USA, 2005.
53. Yelisseyev, A.P.; Isaenko, L.I.; Starikova, M.K. Optical study of defects in lithium iodate α -LiIO₃. *J. Opt. Soc. Am. B Opt. Phys.* **2012**, *29*, 1430–1435. [\[CrossRef\]](#)
54. Sirotin, Y.I.; Shaskolskaya, M.P. *Fundamentals of Crystal Physics*; Nauka: Moscow, Russia, 1975. (In Russian)
55. Moroz, T.N.; Palchik, N.A. The uniqueness of determination of the space group symmetry by means of the vibrational spectroscopy methods. *Crystallogr. Rep.* **2009**, *54*, 734–737. [\[CrossRef\]](#)
56. Rastsvetaeva, R.K.; Tamazyan, R.A.; Pushcharovsky, D.Y.; Nadezhina, T.N.; Voloshin, A.V. K-nenadkevichite, a new representative of the nenadkevichite-labuntsovite series. *Crystallogr. Rep.* **1994**, *39*, 908–914.
57. Rastsvetaeva, R.K.; Tamazyan, R.A.; Pushcharovsky, D.Y.; Nadezhina, T.N. Crystal structure and microtwinning of K-rich nenadkevichite. *Eur. J. Mineral.* **1994**, *6*, 503–509. [\[CrossRef\]](#)

58. Subbotin, V.V.; Voloshin, A.V.; Pakhomovskii, Y.A.; Bakhchisaraitsev, A.Y.; Pushcharovsky, D.Y.; Rastsvetaeva, R.K.; Nadezhina, T.N. Vuoriyarvite $(K,Na)_2(Nb,Ti)_2Si_4O_{12}(O,OH)_2 \cdot 4H_2O$ —A new mineral from carbonatites of the Vuoriyarvi massif, Kola Peninsula. *Dokl. Akad. Nauk* **1998**, *358*, 73–75.
59. Chukanov, N.V.; Pekov, I.V.; Khomyakov, A.P. Recommended nomenclature for labuntsovite-group minerals. *Eur. J. Mineral.* **2002**, *14*, 165–173. [[CrossRef](#)]
60. Chukanov, N.V.; Pekov, I.V.; Zadov, A.E.; Voloshin, A.V.; Subbotin, V.V.; Sorokhtina, N.V.; Rastsvetaeva, R.K.; Krivovichev, S.V. *Minerals of the Labuntsovite Group*; PH Nauka: Moscow, Russia, 2003; 323p. (In Russian)
61. Rastsvetaeva, R.K.; Bolotina, N.B.; Pushcharovskii, D.Y.; Stefanovich, S.Y.; Nadezhina, T.N.; Dimitrova, O.V. $K_4(NbO)_2[Si_8O_{21}]$: Synthesis, structure, and properties. *Crystallogr. Rep.* **1994**, *39*, 915–922.
62. Rastsvetaeva, R.K.; Bolotina, N.B.; Pushcharovskii, D.Y.; Nadezhina, T.N.; Dimitrova, O.V. Modulated crystal structure of $K_4(NbO)_2[Si_8O_{21}]$. *J. Alloys Compd.* **1994**, *209*, 145–150. [[CrossRef](#)]
63. Pushcharovskii, D.Y. New approaches to the XRD studies of complicated crystal chemical phenomena in minerals. *Croat. Chem. Acta* **1999**, *72*, 135–145.
64. Mitchell, R.H. Primary and secondary niobium mineral deposits associated with carbonatites. *Ore Geol. Rev.* **2015**, *64*, 626–641. [[CrossRef](#)]
65. Traversa, G.; Gomes, C.B.; Brotzu, P.; Buraglini, N.; Morbidelli, L.; Principato, M.S.; Ronca, S.; Ruberti, E. Petrography and mineral chemistry of carbonatites and mica-rich rocks from the Araxá complex (Alto Paranaíba Province, Brazil). *An. Acad. Bras. Ci.* **2001**, *73*, 71–98. [[CrossRef](#)]

Publisher’s Note: MDPI stays neutral with regard to jurisdictional claims in published maps and institutional affiliations.



© 2020 by the authors. Licensee MDPI, Basel, Switzerland. This article is an open access article distributed under the terms and conditions of the Creative Commons Attribution (CC BY) license (<http://creativecommons.org/licenses/by/4.0/>).